International Journal of Extreme Manufacturing

TOPICAL REVIEW • OPEN ACCESS

Projection micro stereolithography based 3D printing and its applications

To cite this article: Qi Ge *et al* 2020 *Int. J. Extrem. Manuf.* **2** 022004

View the article online for updates and enhancements.

You may also like

- An adhesive bonding method with microfabricating micro pillars to prevent clogging in a microchannel
Pin-Chuan Chen, Yu-Min Liu and Huang-Chieh Chou
- PROBING THE IONIZATION STATES OF POLYCYCLIC AROMATIC HYDROCARBONS VIA THE 15–20 m EMISSION BANDS
M. J. Shannon, D. J. Stock and E. Peeters
- Underlayer Selection to Improve the Performance of Polycrystalline Ge Thin Film Transistors
Toshifumi Imajo, Kenta Moto, Keisuke Yamamoto et al.

This content was downloaded from IP address 147.8.230.77 on 13/10/2022 at 04:44

OPEN ACCESS
IOP Publishing | IMMT
International Journal of Extreme Manufacturing
Int. J. Extrem. Manuf. **2** (2020) 022004 (19pp)
https://doi.org/10.1088/2631-7990/ab8d9a

Topical Review

Projection micro stereolithography based 3D printing and its applications

Qi Ge[1], Zhiqin Li[2], Zhaolong Wang[3], Kavin Kowsari[4], Wang Zhang[5], Xiangnan He[1], Jianlin Zhou[2] and Nicholas X Fang[4]

[1] Department of Mechanical and Energy Engineering, Southern University of Science and Technology, Shenzhen 518055, Guangdong, People's Republic of China
[2] BMF Material Technology Inc., Shenzhen 518110, Shenzhen, People's Republic of China
[3] State-Key Laboratory of Advanced Design and Manufacturing for Vehicle Body, College of Mechanical and Vehicle Engineering, Hunan University, Changsha 410082, Hunan, People's Republic of China
[4] Department of Mechanical Engineering, Massachusetts Institute of Technology, Cambridge, MA 02139-4307, United States of America
[5] Digital Manufacturing and Design Centre, Singapore University of Technology and Design, 487372, Singapore

E-mail: geq@sustech.edu.cn, zhaolongwang@hnu.edu.cn and nicfang@mit.edu

Received 31 January 2020, revised 6 April 2020
Accepted for publication 26 April 2020
Published 4 June 2020

Abstract

Projection micro stereolithography (PμSL) is a high-resolution (up to 0.6 μm) 3D printing technology based on area projection triggered photopolymerization, and capable of fabricating complex 3D architectures covering multiple scales and with multiple materials. This paper reviews the recent development of the PμSL based 3D printing technologies, together with the related applications. It introduces the working principle, the commercialized products, and the recent multiscale, multimaterial printing capability of PμSL as well as some functional photopolymers that are suitable to PμSL. This review paper also summarizes a few typical applications of PμSL including mechanical metamaterials, optical components, 4D printing, bioinspired materials and biomedical applications, and offers perspectives on the directions of the further development of PμSL based 3D printing technology.

Keywords: projection microstereolithography, multiscale 3D printing, multimaterial 3D printing

(Some figures may appear in colour only in the online journal)

1. Introduction

In contrast to the subtractive nature of conventional machining, additive manufacturing (also known as 3D printing), physically reproduces parallel slices of arbitrary design files by first decomposing the object's shape into a series of parallel slices. 3D printing methods fabricate highly complex 3D objects from computer-aided design (CAD) models by sequentially adding material in the layer-by-layer fashion [1, 2], which minimizes the material waste, and is applicable to a variety of different materials such as polymers, metals, ceramics, composites, and others. Since its invention, various modalities of 3D printing methods have been evolved. New methods are continually presented to overcome challenges encountered in existing methods. So far, in terms of application and market share, 3D printing has spread into various manufacturing areas including electronics, medical, automotive, and aerospace [2]. A report from the United Parcel Service (UPS) and the Consumer Technology Association (CTA) projects forecasts that the 3D printing industry will exceed $21 billion by early 2020s

Original content from this work may be used under the terms of the Creative Commons Attribution 3.0 licence. Any further distribution of this work must maintain attribution to the author(s) and the title of the work, journal citation and DOI.

© 2020 The Author(s). Published by IOP Publishing Ltd on behalf of the IMMT

[3], which supports the notion that continued progress in this sphere is crucial to global economic competitiveness.

Consequently, many 3D printing techniques are now available, which differ in the manner layers that are deposited, operating principles, and the materials scope. The following broad categories constitute the main methods available, some of which are as follows and described below: fused deposition modeling (FDM), direct ink writing (DIW), inkjet, stereolithography (SLA), selective laser sintering/melting (SLS/SLM), two-photon polymerization (TPP) as well as digital light processing (DLP).

Among all 3D printing technologies, fused deposition modelling (FDM) is the most common technology due to its low cost and simplicity [4–6]. In FDM, the heated printing nozzle melts or softens thermoplastic filament and extrude it on a build tray in a layer-by-layer manner to fabricate 3D structures. The extruded filament solidifies due to phase transition (mainly crystallization) after it leaves the heated nozzle.

Similar to FDM, direction ink writing (DIW) is another extrusion-based 3D printing technology [7–12]. Different FDM that uses thermoplastics, a DIW printer deposits viscoelastic inks which are shear thinning materials whose viscosity varies from ~1 kPa s to ~1 Pa s after increasing the pressure from 1/s to 100/s [13]. In order to maintain the desired printed shapes on the build tray, sufficient shear elastic modulus is needed for the thinning materials exiting from the nozzle. For this purpose, thinning agents such as clay need to be added to modify the respective rheological property of inks.

Selective laser melting (SLM) and selective laser sintering (SLS) are two powder- bed-fusion based 3D printing technologies [14–17]. In a SLM/SLS printer, there are fine powders tightly packed in the printing bed. During printing, a laser beam selectively fuses the powders to 2D pattern. The subsequent layer is processed by rolling a layer of powders on top of previous layers and fusing them together. However, it should be noted that SLS is mainly used to process polymers, metals and alloy powders, while SLM is only suitable for certain metals such as steel and aluminum.

Inkjet is a 3D printing method that fabricates 3D structures by using a thermal or piezoelectric technology to deposits nano/microscale low-viscosity ink droplets on a build tray by using [5, 16]. An inkjet printer combines an ink-jetting head and an ultraviolet (UV) light source in one platform. During printing, the ink-jetting head selectively deposits ink droplets on the build tray to form 2D patterns which are immediately solidified upon the illumination of the UV light source.

Different from the above-mentioned 3D printing technologies, the high-resolution 3D printing techniques are realized through localized photopolymerization that precisely transfers liquid polymer resin to solidified voxels. Those high-resolution 3D printing technologies mainly includes two-photon polymerization (TPP) [18–22], stereolithography (SLA) [16, 23–27], digital light processing (DLP) based 3D printing [16, 28–39]. TPP uses an ultrafast pulsed laser to generate a very high flux of photons in a small temporal and spatial volume. Since these photons are at longer wavelengths (780–820 nm), the polymer resin can be solidified only by absorbing two photons at the same time, which allows TPP to achieves sub-micron features [40]. As the first 3D printing technology, SLA was invented in 1986 [41]. In SLA, a rastering laser is used to selectively polymerize a liquid polymer resin in a layer-by-layer manner to fabricate 3D objects. TPP and SLA are both laser-scanning based 3D printing technologies, therefore relatively slow as they locally photopolymerize polymer resin based on point-light-source illumination.

Different from TPP and SLA, DLP based 3D printing performs the localized photo-curing through projecting 2D UV patterns on the surface of liquid polymer resin. DLP that combines the feature of high-resolution with fast-speed. The recent advances in DLP based 3D printing generate various advanced techniques including projection micro stereolithography (PμSL) for high-resolution 3D printing [28–31], continuous liquid interface production (CLIP) for fast-speed 3D printing (1000 mm h^{-1} in the z-direction) [38], as well as high-area rapid printing (HARP) for fast-speed (431 mm h^{-1} in z-direction), large volume 3D printing (38 cm $\times$ 61 cm $\times$ 76 cm in 1 h and 45 min) [39].

Besides the above-mentioned 3D printing technologies which have been widely accepted by the research and industry communities, there are a few emerging technologies that pushes the boundary of 3D printing speed. Electrohydrodynamic (EHD) 3D printing achieves three to four orders of magnitude faster than the other techniques providing equivalent feature sizes [42, 43]. Tomographic volumetric additive manufacturing fabricates a centimeter scale object within tens of seconds, which also indicates consistent advantages of fast speed and high resolution [44, 45]. These technologies will bring 3D printing to a new stage once they are more mature.

In general, there is the contradictory relation between printing area and printing resolution. It means that to print structure with higher resolution needs to reduce the printing area into a smaller one. As shown in figure 1, the above introduced 3D printing technologies offer different printing resolutions, and therefore cover the corresponding printing areas. For example, TPP offers ~100 nm ultrahigh printing resolution [18–22], but it only covers relatively small printing area ranging from 10 μm $\times$ 10 μm to 2.2 mm $\times$ 2.2 mm despite of the recent development of the multiscale printing approach that combines TPP with digital micromirror device (DMD) [22]. In contrast, DIW is a versatile 3D printing technology which can not only be applied to the bio-related 3D printing that covers printing area of 30 mm $\times$ 30 mm with printing resolution of 200 μm [8], but also be used to print constructions in the printing area up to 10 m $\times$ 10 m with the printing resolution of 50 mm [10, 11]. Compared with other 3D printing technologies, DLP based 3D printing technologies cover a broader spectrum of printing resolutions from 0.6 μm to 90 μm by adjusting the magnification of the projection lens. Within the DLP based 3D printing technologies, there is a specific technique termed 'projection micro stereolithography (PμSL)' which is capable of printing complex 3D structures with higher resolution ranging from 0.6 μm to 30 μm and relatively wide printing area up to ~90 mm $\times$ 50 mm [28–31, 36, 46, 47]. The detailed summary of the printing resolution-area relation of different 3D printing technologies is presented in table 1.

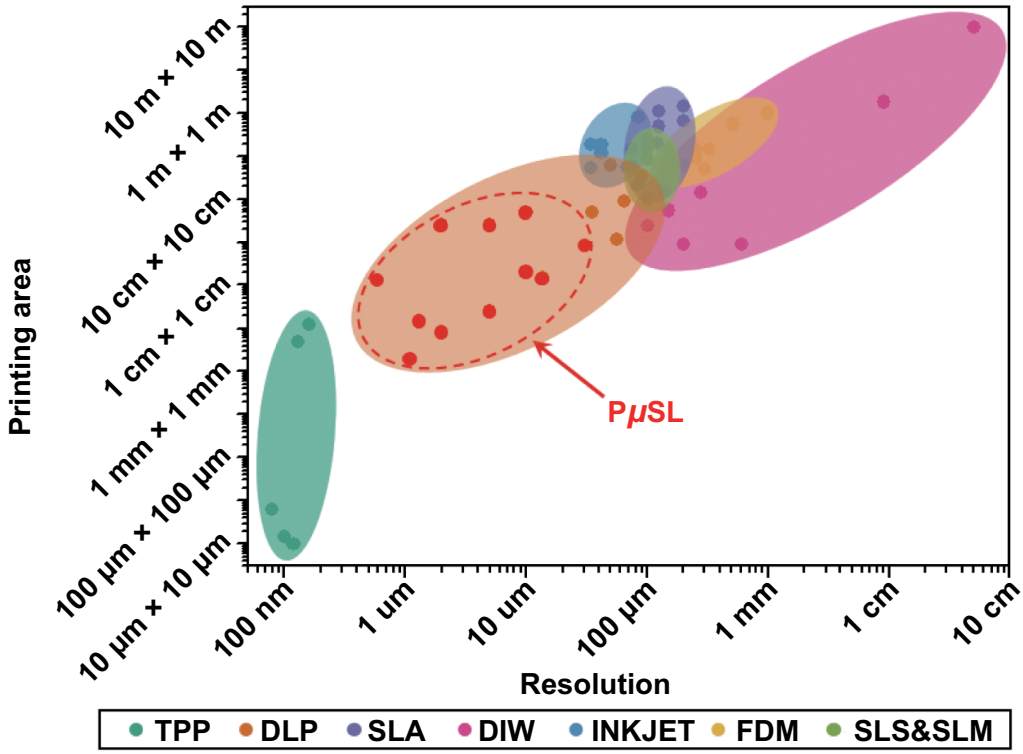

Figure 1. The diagram summarizes the printing resolution and printing area relation of TPP [18–22], DLP [16, 28–39], SLA [16, 23–27], DIW [7–12], inkjet [5, 16], FDM [4–6] as well as SLS&SLM [14–17].

This review paper aims to summarize the recently advanced PμSL based 3D printing technologies. In section 2, we introduce the technological advancements of PμSL based 3D printing including the working principle, commercialized products, and recent developments in multiscale, multimaterial and multifunctional 3D printing. Section 3 summarizes the developments in functional photopolymers that are used in PμSL and other DLP based 3D printing technologies. In section 4, we introduce the typical applications of PμSL based 3D printing including mechanical metamaterials, optical components, 4D printing, bioinspired materials as well as biomedical applications. Finally, section 5 concludes the article and provides perspectives on the directions of the further development of PμSL based 3D printing technology.

2. Pμsl based 3D printing technologies

The early version of high-resolution PμSL apparatus was developed by Sun and his coworkers in 2005 by using the digital micromirror device (DMD) as the dynamic mask [28]. As shown in figure 2(a), the PμSL based 3D printer fabricates a complex 3D microstructure in a layer-by-layer manner. During printing process, a computer aid design (CAD) model is first sliced into a sequence of 2D digital patterns. Then, these 2D patterns are transferred to the DMD chip which modulates the UV light illuminated on it. The shaped UV lights with the corresponding defined 2D patterns pass through a reduction lens that projects the 2D images on the resin surface with a reduced feature size. The patterned UV irradiation triggers the localized photopolymerization on the resin surface, which forms a layer of the printed structure. The translational stages lowers the printing platform, and the UV projection continues to print the subsequent layer. This process proceeds iteratively until the entire structure is fabricated. In order to reveal the underlying mechanisms for PμSL, the authors developed a numerical model based on diffractive optics. The model justified the role of UV doping due to its ability of effectively reducing the curing depth without sacrificing the chemical property of the resin. The first developed PμSL system was able to fabricate highly complex 3D microstructures, such as a microspring array (figures 2(b)), and (a) thread with the feature size as small as 0.6 μm (figure 2(c)).

To further improve the performance of the PμSL system, Zheng *et al* optimized the system design by using liquid crystal on silicon (LCoS) chip as the dynamic mask, and a UV LED as the light source (figure 2(d)) [29]. The authors improved the light projection uniformity by taking advantage of the gray-scale capability of the LCoS spatial light modulator. They carried out the experimental parametric study to investigated the effects of various process control variables, and concluded that the photo absorber concentration and optical intensity are the two most important processing parameters. In addition, the ambient oxygen concentration was precisely controlled by enclosing the UV curable resin bath in an environmental chamber to eliminate the effect of oxygen inhabitation (figure 2(d)). The modified PμSL system is capable of fabricating arbitrary 3D overhanging structures with highly complex geometries such as octet truss unit cell (figure 2(e)) and porous materials (figure 2(f)).

Table 1. Summary of the printing resolution-area relation of different 3D printing technologies.

Technology	Resolution (μm)	Printing area (mm^2)	Reference
TPP	0.08	0.0064	[22]
	0.1	0.000144	[19]
	0.12	0.0001	[20]
	0.13	4.84	[18]
	0.16	12.25	[21]
DLP	0.6	2	[28] (PμSL)
	1.3	15	[29] (PμSL)
	2, 10	8.2944, 2500, 4888	[32] (PμSL)
	5	25	[30] (PμSL)
	5	2500	[31] (PμSL)
	30	768	[36] (PμSL)
	7.6	234.135	[33]
	13.68	147.2451	[34]
	35, 90	5040, 32 969.5	[37]
	56	1161	[35]
	65	8760.96	[16]
SLA	75, 125	62 500, 144 400, 487 500, 1 125 000	[16]
	85, 140	21 025	[27]
	120, 200, 800	202 500, 62 500, 245 000	[25]
	200	1 470 000	[26]
DIW	150	5476	[8]
	200	900	[9]
	600	900	[7]
	9000	1 800 000	[10]
	50 000	100 000 000	[12]
Inkjet	34, 68	52 540, 191 100, 55 130	[16]
	42, 85	116 964, 191 100, 800 000	[5]
FDM	127, 254, 330, 508	64 516, 144 130, 90 170, 144 130, 557 540	[5]
	300	49 200	[4]
	1000	1 010 025	[6]
SLS&SLM	55, 100	9604, 40 000, 84 100	[15]
	100	10 000, 250 000	[16]
	100	160 000	[17]
	140, 150, 500	15 625, 78 400, 140 000, 84 100	[14]

In 2018, a micro/nano fabrication company-BMF Materials Technology Co, Ltd. commercialized the PμSL based 3D printing technologies [32]. It offers two high-resolution large-area printing options: (i) 2 μm per pixel with 50 mm $\times$ 50 mm printing area (nanoArch S130) and (ii) 10 μm per pixel with 94 mm $\times$ 52 mm printing area (nanoArch S140). The system design is presented in figure 3(a). In order to accurately control the layer thickness, a pre-stretched transparent and anti-sticky perfluoroalkoxy (PFA) membrane is placed between the surface of resin and projection lens. Before printing, a high-resolution stage coordinated with a CCD camera automatically moves the membrane to a position where the focal plane of the projection lens coincides with the wet surface of the membrane. The multiple-projection stitching process is adopted to realize large-area printing. The total fabrication area can be further divided into multiple subareas which are smaller than a single projection. When a layer of subarea is printed, the X and Y stages move horizontally for the fabrication of a neighboring subarea. Since its debut, the nanoArch series have been successfully used in various engineering applications including mechanical metameterials (figures 3(b) and (c)), biomedical devices (figures 3(d)–(f)), micro mechanical devices (figures 3(g) and (h)), precision structural parts, and others [32, 48, 49].

To further extend the fabrication capability of the PμSL based 3D printing, several efforts have been made to realize multiscale, multimaterial and multifunctional 3D printing in the past few years. As shown in figure 4(a), Zheng *et al* developed a large area projection microstereolithography (LAPμSL) that combines a traditional DMD based PμSL system with a coordinated optical scanning system [31]. The system combines a galvanometric mirror with a customized scanning lens to project the light pattern from the DMD onto the UV curable polymer resin surface, and therefore is capable of fabricating microstructures with feature size span over four orders of magnitude within only a few hours. Combining LAPμSL with electroless nickel deposition, the authors successfully fabricated the multiscale metallic metamaterials with various 3D features from nanometers to centimeters (figure 4(b)). Inspired by the computer numerically controlled (CNC) accumulation process, Yang *et al* developed another PμSL based multiscale 3D printing approach—immersed surface

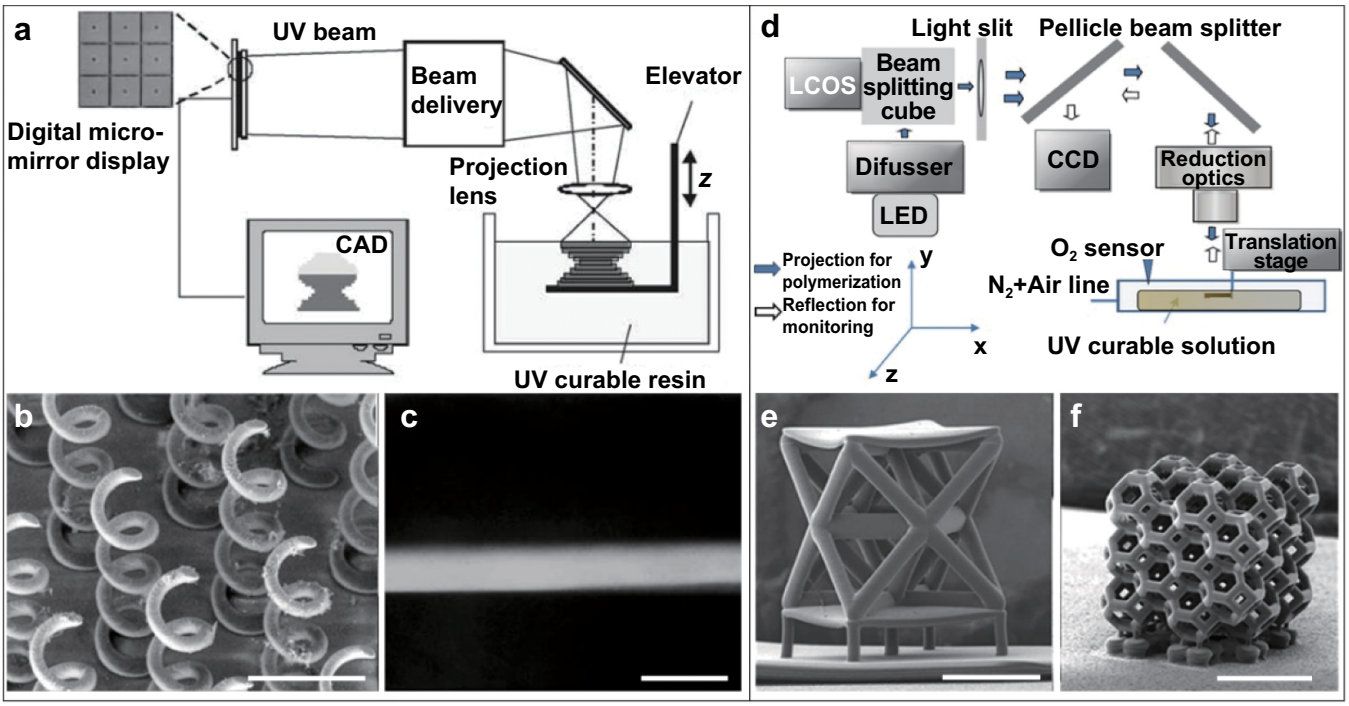

Figure 2. Pμsl based 3D printing technologies. (a)–(c) The first proposed PμSL based 3D printing. Reprinted from [28], Copyright (2005), with permission from Elsevier. (a) Schematic of the system design. (b) micro coil array with the coil diameter of 100 μm and the wire diameter of 25 μm. Scale bar: 200 μm. (c) An ultra fine thread with the diameter of 0.6 μm. (d)–(f) The PμSL system using LCoS chip as the dynamic mask. Reprinted from [29], with the permission of AIP Publishing. (d) Schematic of the system design. (e) Octet-truss unit cell. Scale bar: 490 μm. (f) Porous structure with tetrakaidehedron unit cell architecture. Scale bar: 640 μm.

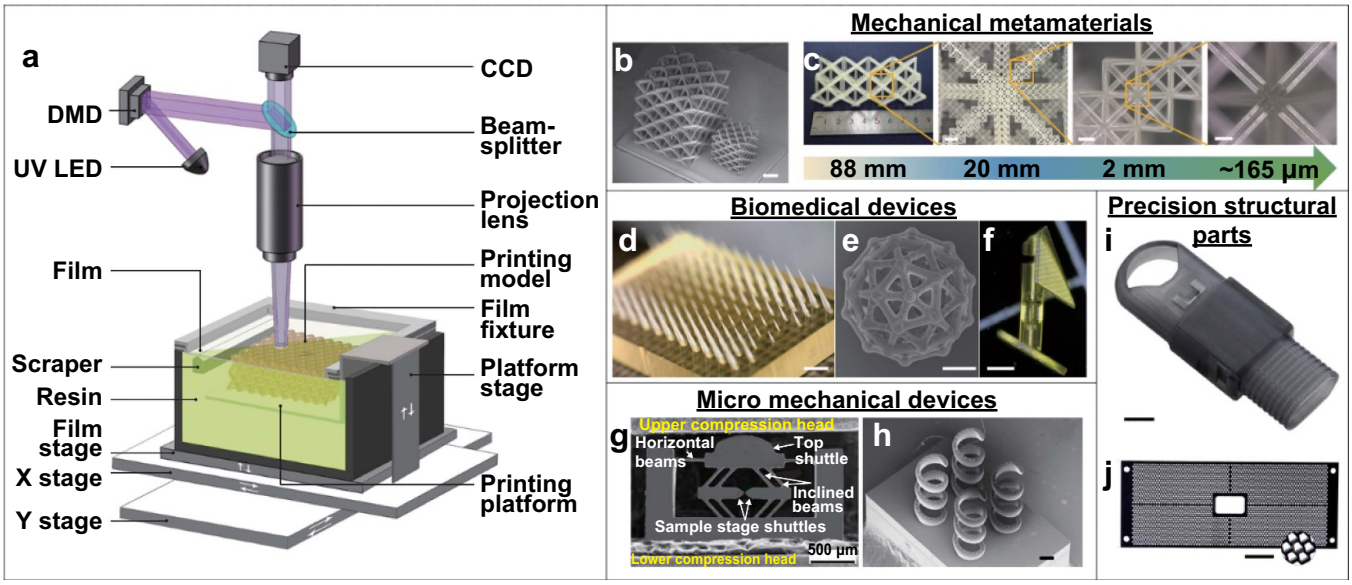

Figure 3. Commercialized high-resolution large-area PμSL based 3D printing system and its engineering applications. (a)–(f), (h)–(j) Reproduced with permission from [32]. (a) Schematics of a PμSL 3D printing system. (b), (c) Application in mechanical metamaterials. (b) The printed mechanical metamaterial in the octet truss form. Scale bar: 100 μm. (c) The mechanical metamaterial in the hierarchical structure form. Scale bars from left to right: 2 mm, 200 μm, and 500 μm respectively. (d)–(f) Application in biomedical devices. (d) Tilted microneedles for drug injection. Scale bar: 1 mm. (e) Micro buckyball for cell cultivation. Scale bar: 50 μm. (f) Drainage nail for glaucoma. Scale bar: 500 μm. (g), (h) Micro mechanical devices (MMDs). (g) A MMD for *in-situ* tensile testing of micro/nanowires. Reprinted from [50], Copyright (2019), with permission from Elsevier. (h) Micro spring array with 20 μm diameter for each spring. Scale bar: 100 μm. (i), (j) Precision structural parts. (i) Micro fiber connector with minimum groove edge thickness of 80 μm. Scale bar: 5 mm. (j) Micro socket with approximately 1700 trapezoidal hole arrays. Scale bar: 12.5 mm.

accumulation based 3D (ISA-3D) printing where the light guide tool consisting of optical fibers and objective lens is the key component (figure 4(c)) [51]. The light guide tool is merged inside a tank of UV curable resin for continuous

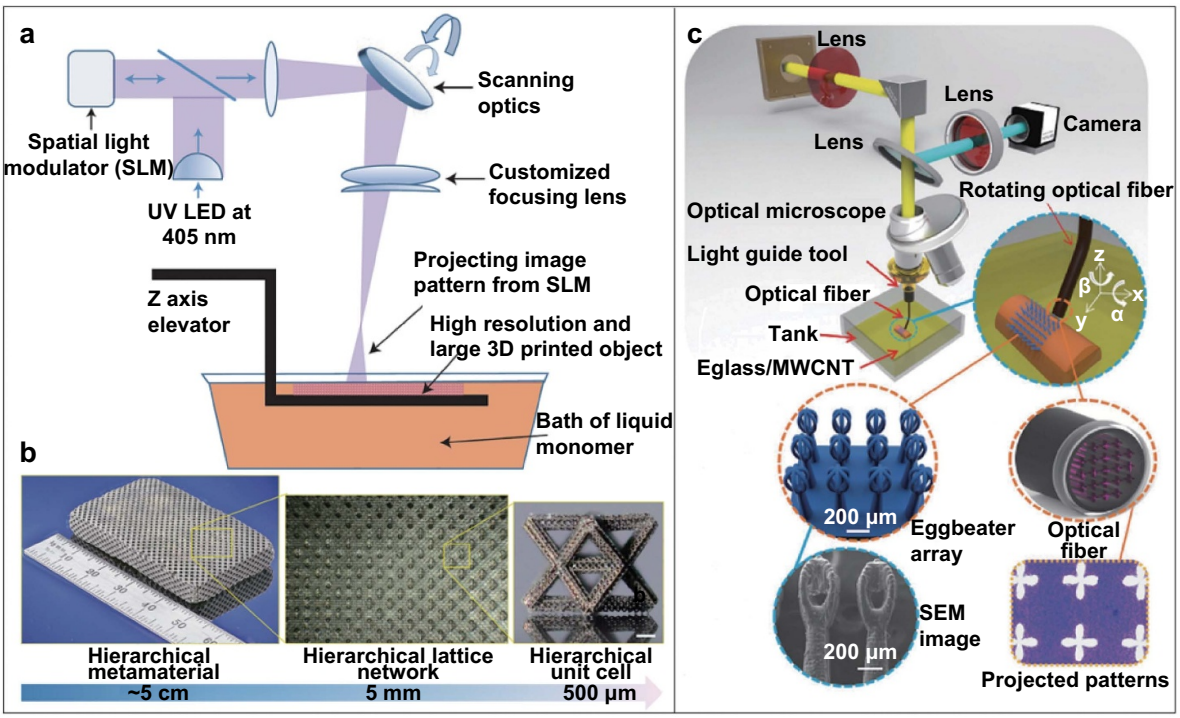

Figure 4. Pμsl based multiscale 3D printing. (a), (b) Large area projection microstereolithography (LAPμSL) multiscale 3D printing. Reprinted by permission from Macmillan Publishers Ltd: Nature Materials [31], Copyright (2016). (a) Schematic of the LAPμSL printing system that combines a traditional DMD based PμSL system with a coordinated optical scanning system. (b) Snapshots of a hierarchical mechanical metamaterial. Scale bar is 80 μm. (c) Schematic illustrations of the ISA-3D printing system. Inserts show the magnification of light guide tool, optical fiber with projected 2D micro patterns, models and SEM image of the 3D-printed eggbeater arrays. [51] John Wiley & Sons. © 2017 WILEY–VCH Verlag GmbH & Co. KGaA, Weinheim.

2D light beam projection. Combining with the 5-axis movement of the light guide tool and the dynamically controlled light beam projection, the ISA-3D printing system enables the fabrication of microscale features on the surface of a macroscale object. It is capable of projecting UV patterns on a 3.67 mm $\times$ 2.75 mm with resolution of 2.5 μm per pixel. Using the ISA-3D system, the authors successfully printed bioinspired super-hydrophobic structure with 2.5 μm feature size on centimeter scale curved surface.

Multimaterial 3D printing is a desired capability which allows users to fabricate heterogenous 3D structures that have the inaccessible functionalities by single material printing such as 4D printing [36, 52, 53], negative thermal expansion [54], organ-like structures [55], and others [56–58]. Among all the 3D printing technologies, the multimaterial fabrication can be easily realized in FDM and DIW through simply adding extra printing nozzles to deposit different materials, and inkjet 3D printing technology in which photocurable resin is jetted over a surface through micro-nozzles followed by curing with UV light. However, compared with the above discussed 3D printing technologies, the development of multimaterial PμSL based 3D printing systems remain comparatively limited due to the difficulties of exchanging polymer resins [46, 47]. To address this, Kowsari *et al* built a high-resolution, high-speed, and high-efficiency PμSL based multimaterial 3D printing system that used a translationally moved glass plate to deliver different material puddles to realize the fast-speed material exchange, and employed an air jetting based cleaning step to minimize the degree of resin waste and material contamination, and avoid the use of any cleaning solutions which damage the printed parts [46]. Figure 5(a) describes the efficient material-exchange mechanism where the glass plate also serves to deliver various material puddles to the printing platform to enable the multimaterial printing. During material exchange, the air jetting is applied to blow away the residual resin on the printed structure to minimize the degree of material contamination during material exchange. The developed system enables the fabrication of high-resolution complex 3D structures with 15 μm feature size and the sharp transition between two materials (figure 5(b)). Besides, Han *et al* developed a rapid multi-material PμSL 3D printing system that utilizes the dynamic fluidic control of multiple liquid photopolymers within an integrated fluidic cell to fabricate highly complex multimaterial 3D microstructures through a rapid multimaterial exchange process [47]. As shown in figure 5(c), the rapid material exchange between liquid photopolymers takes place in the sealed fluidic cell which even allows to exchange micro-/nano-particle suspensions leading to 3D printing of heterogeneous structures of metallic/ceramic, and even biomedical materials (figure 5(d)).

Instead of directly exchanging materials during printing process, printing structures using polymer solution loaded with nano/micro particles or fibers is another efficient way to fabricate multimaterial structures. The key to realize

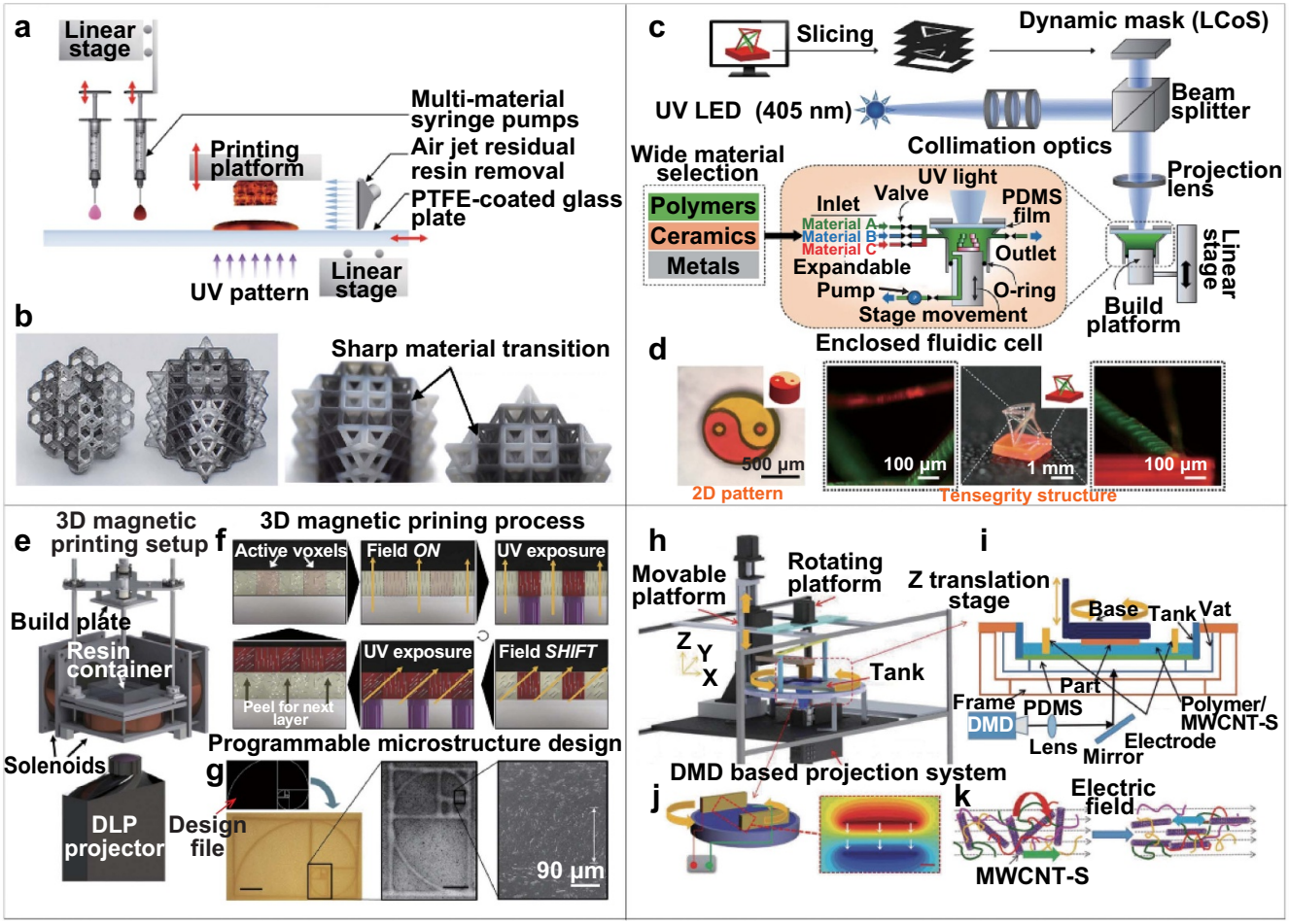

Figure 5. Pμsl based multimaterial 3D printing systems. (a), (b) Air jetting assisted multimaterial 3D printing system. Reproduced with permission from [46]. (a) Schematic of the material exchange mechanism. (b) Photographs of printed multimaterial structures with high resolution and sharp material transition. (c), (d) Dynamic fluidic control based rapid multimaterial 3D printing system. Reprinted from [47], Copyright (2019), with permission from Elsevier. (c) Schematic illustration of the fluidic controlled multimaterial printing system. (d) Optical microscope images of the printed multimaterial structures. (e)–(g) 3D magnetic printing system. Reproduced from [59]. CC BY 4.0. (e) Schematic of the printing system. (f) Illustrations of printing process. (g) 3D magnetic printing micro-architectures with clear feature sizes as low as 90 μm. Scale bar, 2 mm, 500 and 50 mm in (c) from left to right. (h)–(k) Electrically assisted printing system. [60] John Wiley & Sons. © 2017 WILEY–VCH Verlag GmbH & Co. KGaA, Weinheim. (h) Diagram of electrically assisted 3D-printing device. (i) A bottom-up projection process. (j) Two parallel electrodes with applied DC electric field. (k) Schematic diagram shows rotation of CNT in polymer resin under the application of electric field.

multimaterial 3D printing based on this approach is to precisely manipulate the particle/fiber orientation through external assistive fields. As shown in figure 5(e), Martin *et al* developed a 3D magnetic printing system that integrates the real-time colloidal assembly into a usual DLP 3D printing system [59]. The system can finely tune the direction of the ceramic-reinforcing particles within each individual voxel, thus is able to printing dense ceramic/polymer composites where the orientations of the discontinuous ceramic fibers are well defined. In order to make the ceramic particles magnetic field responsive, iron oxide nanoparticles were coated to those nonmagnetic-reinforcing materials (such as alumina, silica and calcium phosphate). During printing, the reinforcing microparticles/fibers are aligned upon the application of a rotating magnetic field. Then, PμSL system polymerizes the voxels with aligned particles to solidify the structure and fix the orientation of the reinforcement (figure 5(f)). The two steps are repeated until the printing of a layer with different particle orientations is completed. Using the 3D magnetic printing system, the authors successfully printed complex bioinspired reinforcement structures with enhanced material properties (figure 5(g)). Instead of using magnetic field, Yang *et al* developed an electrically assisted 3D printing system that is capable of fabricating bioinspired reinforcement architecture where the multiwalled carbon nanotubes (MWCNT-S) are dynamically aligned by applying a rotating electrical field [60]. As depicted in figures 5(h)–(j), DC voltages were applied on two parallel plate electrodes to generate the parallel electric field that controls the orientation of the MWCNT-S. The research found that torque, coulombic and electrophoresis forces dominate the rotation of carbon nanotubes. The electric field generates polarization of CNT resulting in a torque force (red arrow in figure 5(k)). Oppositely charged ends of different CNTs generate coulombic attraction (blue arrow in figure 5(k)). The charged surface produce electrophoresis force (green arrow in figure 5(k)). Using the electrically

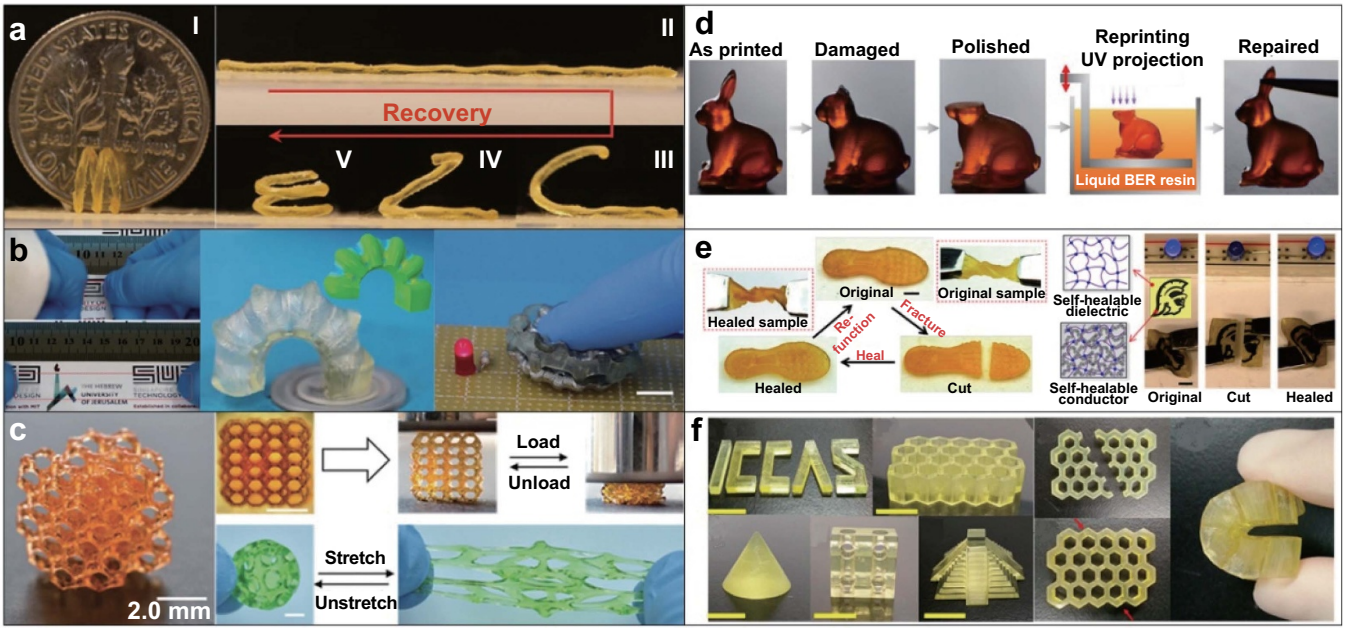

Figure 6. High performance multifunctional photopolymer for PμSL based 3D printing. (a) Highly deformable shape memory polymer for 4D printing. Reproduced from [36]. CC BY 4.0. (b) Highly stretchable and UV curable elastomer. [66] John Wiley & Sons. © 2017 WILEY–VCH Verlag GmbH & Co. KGaA, Weinheim. (c) Highly stretchable and UV curable hydrogel. Reproduced from [56] with permission of The Royal Society of Chemistry. (d) Reprocessable thermosets for sustainable 3D printing. Reproduced from [67]. CC BY 4.0. (e) Self-healing elastomer for additive manufacturing. Reproduced from [68]. CC BY 4.0. (f) Self-healing polyurethane elastomers for 3D printing. Reprinted with permission from [69]. Copyright (2019) American Chemical Society.

assisted 3D printing system, the authors successfully fabricated mechanically enhanced artificial meniscus with radial and circumferential aligned MWCNT-S. Moreover, they also used this system to print nacre-inspired hierarchical structures with electrically aligned graphene nanoplatelets (GNs) acting as bricks within the polymer matrix as mortar [61].

3. 3D printing materials

A PμSL system prints 3D structures through free-radical photopolymerization which converts liquid photopolymer resin consisting of small molecules including monomers, crosslinkers, oligomers to covalently crosslinked solid. (Meth)acrylate monomers/oligomers are the most widely used polymer resins for photopolymerization based 3D printing processes. The photopolymerization is a free radical based polymerization, and includes four main steps: radical generation, initiation, propagation, and termination [62, 63]. In early days, poly(ethylene glycol) diacrylate (PEGDA) and 1,6-hexanedioldiacrylate (HDDA) were the two mainly used UV curable resins for the PμSL based 3D printing system [28, 29]. Simple functionalities can be easily achieved by doping nano/micro particles or fibers into photopolymers. For example, Mu *et al* imparted the electric conductivity into 3D printed structure by mixing photocurable resin with multi-walled carbon nanotubes [64]; Wang *et al* tuned the stiffness and thermal expansion coefficient of printed structure by adding copper nanoparticles into the photocurable resins [54]; Zhang *et al* made the 3D printed structures self-healable by dissolving polycaprolactone (PCL) into the photopolymers [65]. Moreover, one can use the printed polymer structure as template to transfer the polymer-based structures to metallic and ceramic ones. A metallic micro lattice structure can be fabricated via electroless nickel plating [30, 31]. The thickness of the metal coating can be controlled from 100 nm to 2 μm. A hollow-tube aluminum oxide microlattices can be produced by atomic layer deposition (ALD) that controls the alumina thicknesses from ~40 to 210 nm [30]. One can print solid ceramic lattices by loading aluminum oxide nanoparticle into photopolymer resin, and sintering the printed polymeric structures [30].

In recent years, researchers developed a variety of novel (meth)acrylate based UV curable polymers to meet the requirements of different applications. For example, Ge *et al* reported a highly tailorable and deformable 4D printing shape memory polymer system consisting of benzyl methacrylate (BMA) as monomer and bisphenol A ethoxylate dimethacrylate (BPA) as crosslinker [36]. The 3D structure printed with the BMA-BPA can be deformed by up to 300% (figure 6(a)). In order to extend the ability of PμSL to fabricate soft and flexible 3D structures and devices such as soft robots, mechanical metamaterials as well as flexible electronics, Patel *et al* developed highly stretchable and UV Curable (SUV) elastomers by mixing the monomer-epoxy aliphatic acrylate (EAA) with the crosslinker—aliphatic urethane diacrylate (AUD) [66]. The energy dissipation resulting from the breakage of a certain hydrogen bonds between C = O groups and N-H groups of AUD leads to the highly stretchability of the SUV elastomer system which can be stretched by up to 1000% and used to directly 3D print soft actuators and flexible electronics (figure 6(b)). In addition, Zhang *et al* developed a UV curable and highly stretchable hydrogel system by

using a method to convert non-water soluble photo-initiator, 2,4,6-trimethylbenzoyl-diphenylphosphine oxide (TPO) water soluble [56]. This approach makes the acrylamide-PEGDA hydrogel system compatible with PμSL based 3D printing system, therefore enables the fabrication of high-resolution hydrogel structures with large deformation (up to 1300%) (figure 6(c)).

The photopolymers that are compatible with PμSL and other DLP based 3D printing technologies are thermosets which are not repairable after damage due to permanent covalent bonds formed during photopolymerization. In order to impart the self-healing capability to the conventionally unrepairable photopolymers, several efforts have been made. Zhang *et al* reported a two-step polymerization strategy to develop 3D printing reprocessable thermosets (3DPRTs) [67]. In the 3DPRT solution, acrylate functional groups are UV reactive, therefore compatible with PμSL based 3D printing, and a the heating triggered transesterification reaction between the hydroxyl and ester functional groups generates dynamic covalent bonds that impart reprocessability into printed structures. The developed 3DPRTs makes the PμSL printed 3D structures reshapable, repairable, and recyclable (figure 6(d)). Instead of using transesterification reaction, Yu *et al* developed a type of UV curable self-healing elastomers that contain both thiol and disulfide groups. In the self-healing elastomer system, the thiol functional group leads to the thiol-ene photopolymerization during UV curing, and the disulfide group results in a disulfide metathesis reaction during self-healing process [68]. To demonstrate both 3D printing and self-healing capability, the authors printed a shoe pad sample which can be twisted by 540°. A damaged shoe which was healed for 2 h at 60 °C could recover the capability of the 540° twisting (figure 6(e)). In order to further improve the stretchablility of the self-healing elastomers, Li *et al* reported a type of the stretchable self-healing elastomer made of polyurethane [69]. The authors first synthesized polyurethane acrylate with disulfide bonds, and then compounded it with reactive diluent and photoinitiators to prepared the UV curable solution. The developed self-healing polyurethane elastomer shows excellent stretchablity (up to 400%) and healing efficiency (95% of mechanical recovery) (figure 6(f)).

4. Applications of PμSL based 3D printing

4.1. Mechanical metamaterials

Metamaterials are artificial materials with properties that do not exist in nature, and extend beyond natural materials. A metamaterial gains these properties from its structure rather than from the materials it is composed of. The applications of metamaterial evolve from electromagnetic materials [70–72], to elastic [73], acoustic [74, 75], as well as structural materials [30, 31].

In 2014, Zheng *et al* first used the term 'mechanical metamaterials' which refers to a group of materials with mechanical properties are dominated by their geometry instead of their composition [30, 31]. In general, the mechanical properties of ordinary materials degrade rapidly with the decrease in material density because of the bending-dominated microarchitectures (figures 7(a)–(c)). Using PμSL based high-resolution 3D printing, Zheng *et al* developed a class of ultra-light, ultra-stiff mechanical metamaterials that keep a nearly constant stiffness per unit mass density, even at ultra-low material density. The micro-architectured materials were formed with octet-truss based microscale unit cells which are stretching-dominated (figures 7(d)–(f)), and made of polymers, metals or ceramics combined with postprocessing and nanoscale coating. Compared with those previously reported ultralight materials, the mechanical metamaterial reported by Zheng *et al* exhibit marvelous high stiffness across more than three orders of magnitude in material density (figure 7(g)).

Furthermore, Zheng *et al* built the LAPμSL (figure 4(a)) to fabricate scalable metamaterials with hierarchical microarchitectures [31]. In addition, the authors employed electroless nickel deposition to the metallic nanoscale hollow tube. As presented in figure 7(h), the disparate 3D features span from nanometers to centimeters. By using the fractal hierarchical designs, the relative density of such kind of scalable metamaterials made of nickel-phosphorus can be varied in the range of 0.012%–0.1%. More importantly, the nickel-phosphorus metamaterials can be compressed and stretched with respectively of a scale around 50% and 20%. The unique tensile strength of the nickel 3D scalable hierarchical metamaterials proposed can be as high as 40.8 MPa g^{-1} cm^3 much greater than that of those previously reported structures (figure 7(i)). The remarkable mechanical performances of the hierarchical nickel metamaterials come from the rotation of the nodes of the second-order bend dominated hierarchical ligaments. Most significantly, the strength-density scaling relation of such kind of 3D metamaterials can be adjusted by changing the topologies at all the nanoscale, microscale, as well as centimeter scale levels.

Besides high stiffness, the negative thermal expansion (NTE) is another extraordinary mechanical property that is expected in many engineering applications where the thermal stress mismatch is significant including such as microchip devices, dental filling, adhesive fillers, as well as high precision mechanical or optical devices that work under the varying-temperature conditions [54]. To realize NTE lightweight materials, Wang *et al* used the wheel-driven, droplet-delivery multimaterial PμSL 3D printing to fabricate the metamaterial structures consisting of two different materials with different thermomechanical properties. As presented in figure 7(j), the green beam frame is made of PEGDA, while these black beams are made of PEGDA loaded with copper nanoparticles. The existence of the copper nanoparticles greatly lowers the thermal expansion coefficient (TEC) of the PEGDA composite. With special designed microstructures shown in figure 7(j), the green beams expand more than the black beams due to the different TECs, while the black beams bend inward, leading to a fact that the structure shrinks when heated. It can be seen from figures 7(k) and (l) that the printed mechanical metamaterial exhibits the negative thermal expansion behavior in a broad temperature spectrum ranging from 350 to 520 K.

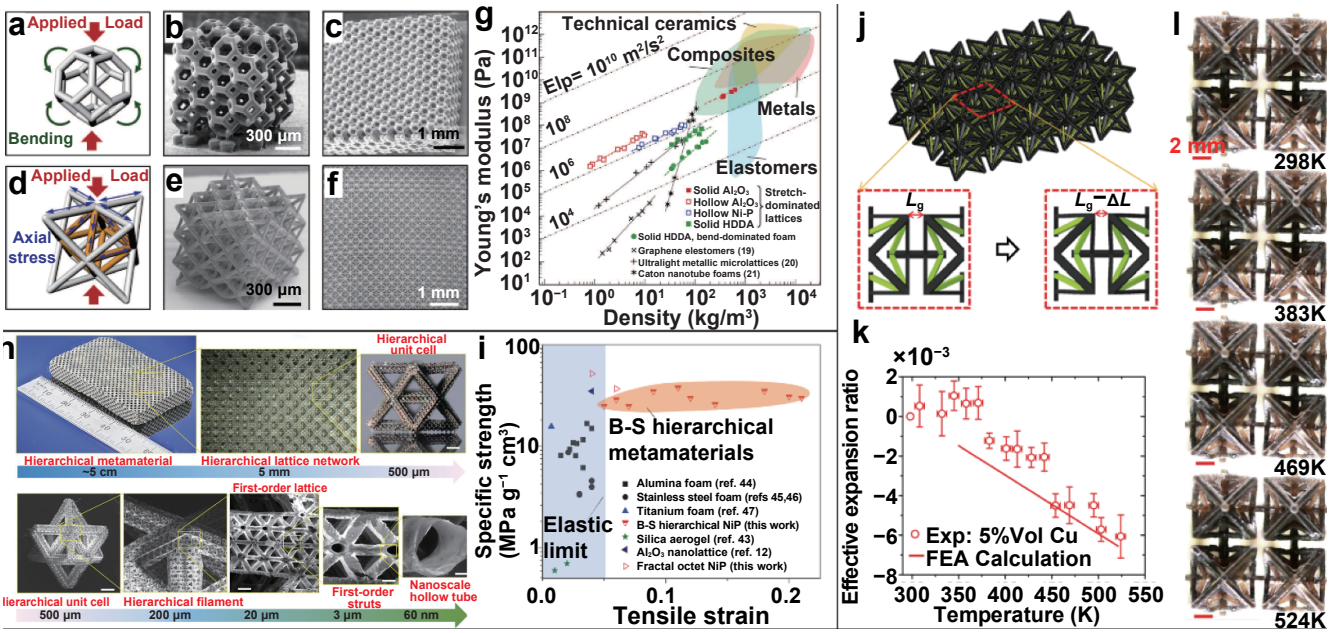

Figure 7. Mechanical metamaterials. (a)–(g) Ultralight, ultrastiff mechanical metamaterial. Reprinted by permission from Macmillan Publishers Ltd: Nature Materials [31], Copyright (2016). (a) Mechanical response to compressive loading of a bending-dominated tetrakaidecahedron unit cell. (b) Tetrakaidecahedron unit cell packed into a cubic benddominated lattice (Kelvin foam). (c) SEM image of a bend-dominated lattice composed of a network of tetrakaidecahedron unit cells. (d) Mechanical response to compressive loading of a stretch-dominated octet-truss unit cell. (e) Octet-truss unit cells packed into a cubic microlattice. (f) SEM image of a stretch-dominated lattice material composed of a network of octet-truss unit cells. (g) An Ashby chart plotting compressive stiffness versus density for ultralight, ultrastiff mechanical metamaterials and other previously reported materials. (h), (i) Multiscale metallic metamaterials. From [39]. Reprinted with permission from AAAS. (h) Nickel alloy hierarchical metamaterial and critical features across seven orders of magnitude in length scale. (i) Specific ultimate tensile strength versus elongation to fracture of hierarchical bend–stretch lattice material compared with non-hierarchical stretch-dominated nickel lattices and literature data on low-density metal alloys. (j)–(l) Lightweight mechanical metamaterials with tunable negative thermal expansion. Reprinted figure with permission from [54], Copyright (2016) by the American Physical Society. (j) Illustration of NTE metamaterial design. (k) Experimentally observed and computationally calculated effective expansion ratios. (l) experimental sequences of a 2 by 2 composite lattice under raising temperature.

4.2. Optical components

The conventional methods used to fabricate optical components are costly and time-consuming. Therefore, to simplify the fabrication process and enrich the fabrication capability, researchers have made efforts to apply 3D printing to the fabrication of optical components [76]. Employing femtosecond TPP, Gissibl *et al* successfully fabricated multi-lens objectives with a minimum size around 100 μm [77]. However, point-by-point scanning mechanism determines the fabrication time proportional to (dimension/voxel size)^3, and results in the fact that the femtosecond TPP is not practical to fabricate millimeter-sized optical elements as the fabrication time takes weeks [76].

To develop a time- and cost-effective 3D printing technique for customized optical components, Chen *et al* proposed a highly parallel PμSL process that the grayscale photopolymerization works in coordination with the meniscus equilibrium post-curing methods to achieve the subvoxel-scale accuracy with a deep subwavelength surface smoothness [76]. The proposed approach enables the 3D printing of customized aspheric lenses with optically smooth surface, and high optical performance. As shown in figures 8(a)–(d), to avoid the inherent staircase roughness resulted from additive manufacturing process, the authors compared the meniscus equilibrium post-curing method as well as the grayscale polymerization method which both failed to create a 5 mm spherical lens with optically smooth surface (figures 8(b) and (c)). After combining these two approaches together, the authors successfully fabricateed lenses where the staircase roughness were successfully removed and the image quality was greatly enhanced (figure 8(d)). The results demonstrate that the PμSL process has the potential to fabricate lenses with subwavelength surface smoothness (7 nm) without sacrificing the fabrication speed [76]. This approach enables users to complete the fabrication of customized aspheric lens 5 mm in height and 3 mm in diameter in four hours. The 3D printed singlet aspheric lens demonstrates high quality including 373.2 lp mm^{-1} maximal imaging resolution and less than 0.13% field distortion across a 2 mm field of view. To further demonstrate an application example, the authors attached the 3D-printed aspheric singlet lens to a cell phone (figure 8(e)) which successfully captured the colorful fine details of a sunset moth's wing (figures 8(f) and (g)) and the spot on a weevil's elytra.

To further improve the surface roughness resulted from the pixelated projection of PμSL, and simplify the fabricate process, Yuan *et al* proposed an oscillation-assisted PμSL based 3D printing method to fabricate microlens arrays with

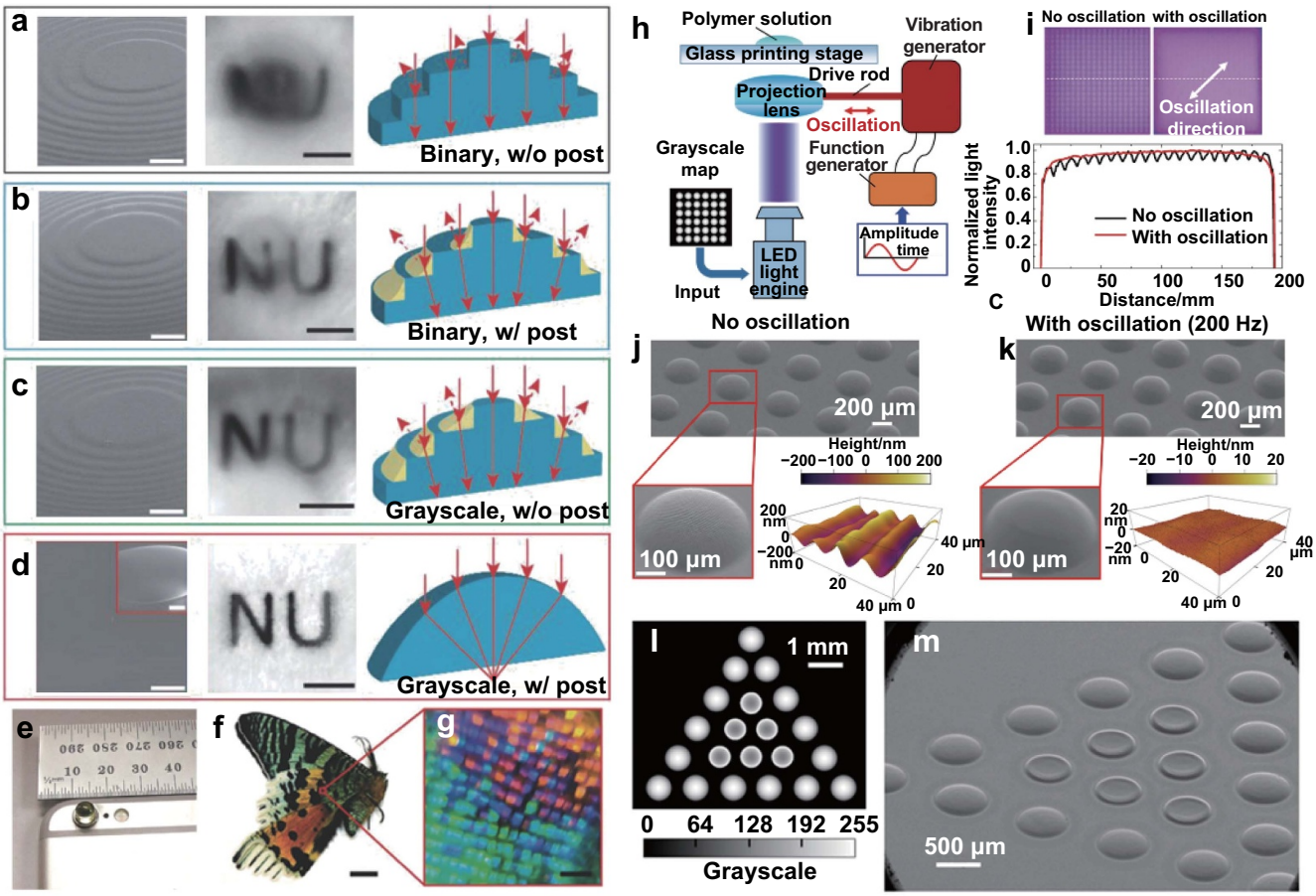

Figure 8. PμSL based 3D printing optical components. (a)–(e) Grayscale PμSL combied with the meniscus equilibrium post-curing process. [76] John Wiley & Sons. © 2018 WILEY–VCH Verlag GmbH & Co. KGaA, Weinheim. (a) Lens printed by binary patterns without post-curing process. (b) Lens printed by binary patterns and the following meniscus equilibrium post-curing process. (c) Lens printed by grayscale photopolymerization without the meniscus equilibrium post-curing process. (d) Lens printed by grayscale photopolymerization and the following meniscus equilibrium post-curing process. Scale bars: 200 μm for the first column (a)–(d), 1 mm for the inset of (d). Scale bars: 1 mm for the second column in (a)–(d). (e)–(g) Demonstrations of low-cost optical microscopy using a 3D-printed aspheric lens. (e) Photograph of an aspheric lens attached to a cell phone camera. (f) Photograph of a Madagascan sunset moth. Scale bar: 20 mm. (g) Recorded image of the moth's wing taken by phone camera with a printed lens. Scale bar: 500 μm. (h)–(m) Oscillation-Assisted grayscale PμSL printing of microlens array. Reprinted with permission from [78]. Copyright (2019) American Chemical Society. (h) Schematic of the oscillation-assisted PμSL -based printing system. (i) Comparison of the projection pattern and normalized light intensity distribution between nonoscillated and oscillated projection. (j), (k) Scanning electron microscopy (SEM) and atomic force microscopy (AFM) characterizations of the microlens arrays fabricated under nonoscillated and oscillated projection. (l) Grayscale map with the hybrid grayscale design. (m) SEM image of the hybrid microlens array.

optically smooth surface through a single 1–3 s exposure of grayscale UV light (figure 8(h)) [78]. Computationally designed grayscale patterns are applied to realize microlens profiles via one single UV exposure that eliminates the staircase effect existing in the traditional layer-by-layer 3D printing fashion. To further remove the jagged surface formed from the gaps between the discrete pixels, mechanical oscillation is employed to the projection lens (figure 8(i)). By combining the single grayscale UV exposure with the mechanical oscillation, the authors successfully achieved the printed microlenses with about 1 nm surface roughness of printed microlenses (figures 8(j) and (k)). Moreover, using the method, users can print microlenses with various curvatures and profiles via one single exposure by taking a advantage of the flexibility of DMD based UV pattern irradiation (figures 8(l) and (m)).

4.3. 4D printing

'4D printing', an emerging 3D printing technology that creates 3D structure whose configuration can change over the fourth dimension-'time' in response to environmental stimuli, was firstly proposed by Tibbits at a 2013 TED Talk [79]. Soon after, the first research paper on 4D printing was published in 2013 by using the concept of printed active composites (PACs) where a printed composite sheet can transform into a complex geometry upon heating due to the shape memory effect of the printed shape memory fibers [52]. 4D printing is realized by 3D printing structures that are made of soft active materials (SAMs) which could actively perform large deformation in response to environmental stimulus such as heat, moisture, light, electric current, voltage, magnetic field and others. The most commonly used SAMs include shape memory polymers

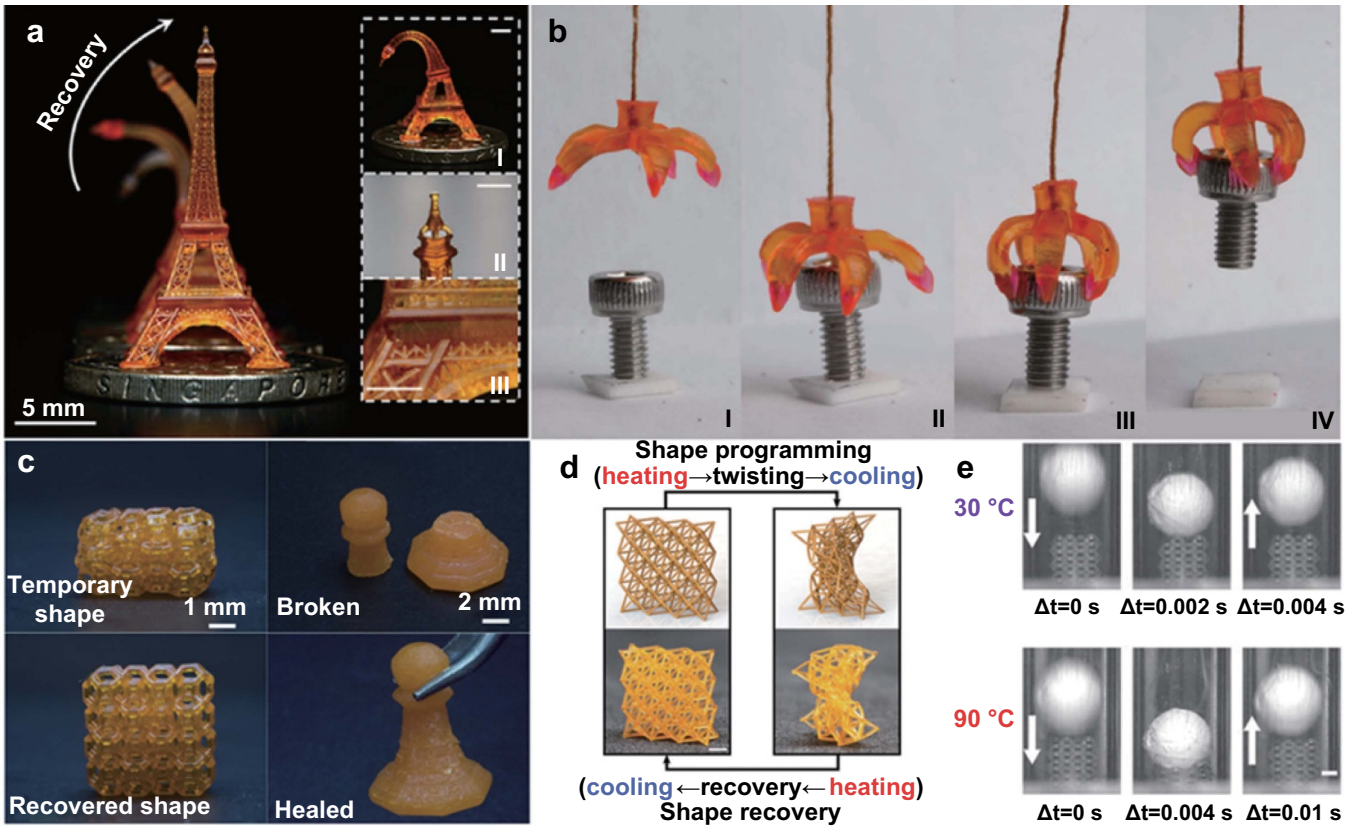

Figure 9. Pμsl based high resolution 4D printing. (a), (b) Highly tailorable (meth)acrylate SMP based 4D printing. Reproduced from [36]. CC BY 4.0. (a) A 4D printed Eiffel tower. (b) A 4D printed multimaterial gripper. (c) Self-healing 4D printing. Reprinted with permission from [65]. Copyright (2019) American Chemical Society. (d)–(e) 4D printing reconfigurable, deployable and mechanically tunable metamaterials. (d) A typical shape memory cycle of a SMP microlattice. Reproduced from [83] with permission of The Royal Society of Chemistry. Shape programing through heating, deformation and cooling, and shape recovery to its original shape upon heating. Scale bar is 2 mm. (e) Time-lapsed images of the Kelvin foam sample during an impact loading at 30 °C and 90 °C. Scale bars are 3 mm.

(SMPs) [36, 52, 53, 80–83], hydrogels [8, 84, 85], liquid crystal elastomers [86–89].

The early attempts on 4D printing mainly relied on a commercial multimaterial PolyJet 3D printer (ObJet, Stratasys, MN, USA) which has the limitations including low mechanical performance of the printing materials provided by the supplier, untailorable 3D printing materials, and relatively low planar printing resolution (~200 μm) [90]. To address those limitations, Ge *et al* developed a highly tailorable (meth)acrylate based SMPs which are UV curable, thus comparable with PμSL based high resolution 3D printing. The (meth)acrylate based SMPs have high tailorablility allowing users to freely tune thermomechanical properties such as glass transition temperature (T_g), rubbery modulus as well as failure strain by choosing different monomers, crosslinkers, and tuning the molecular weight of crosslinkers and the mixing ratio between monomer and crosslinker [36]. The research found that the SMP system with 90% of Benzyl methacrylate (BMA) as monomer and 10% of bisphenol A ethoxylate dimethacrylate (BPA) exhibit high deformability and can be stretched by more than 300%. The high deformability and compatibility with PμSL based 3D printing enables the 4D printing with large deformation and high resolution which was reflected by high resolution bent Effiel tower in figure 9(a). Moreover, the authors used multimaterial PμSL based 3D printing to print a micro gripper where the hinges were printed with SMP and the tips were printed with a soft material whose modulus can be adjusted based on the modulus of the target object (figure 9(b)). In addition, to make the chemically crosslinked SMP network self-healable, Zhang *et al* developed a UV curable double-network SMP system for self-healing 4D printing [65]. In this system, benzyl methacrylate (BMA) works as monomer, and poly(ethylene glycol)-dimethacrylate (PEGDMA) serves as crosslinker to form a 3D printable and highly deformable SMP network; polycaprolactone (PCL) working as self-healing agent is incorporated into the network system to impart the self-healing ability to the 4D-printed structures (figure 9(c)).

Instead of using Benzyl methacrylate as monomer, Yang *et al* developed a UV curable SMP solution that uses acrylic acid (AA) as monomer and bisphenol A ethoxylate dimethacrylate (BPA) as crosslinker to print lightweight metamaterials with reconfigurable geometries, deployable functions, as well as tunable mechanical properties [83]. The printed high-resolution complex metamaterial structures can be programmed into different shapes and recover to the original shape following a shape memory cycle (figure 9(d)). More importantly, due to the transition from glass state to rubbery

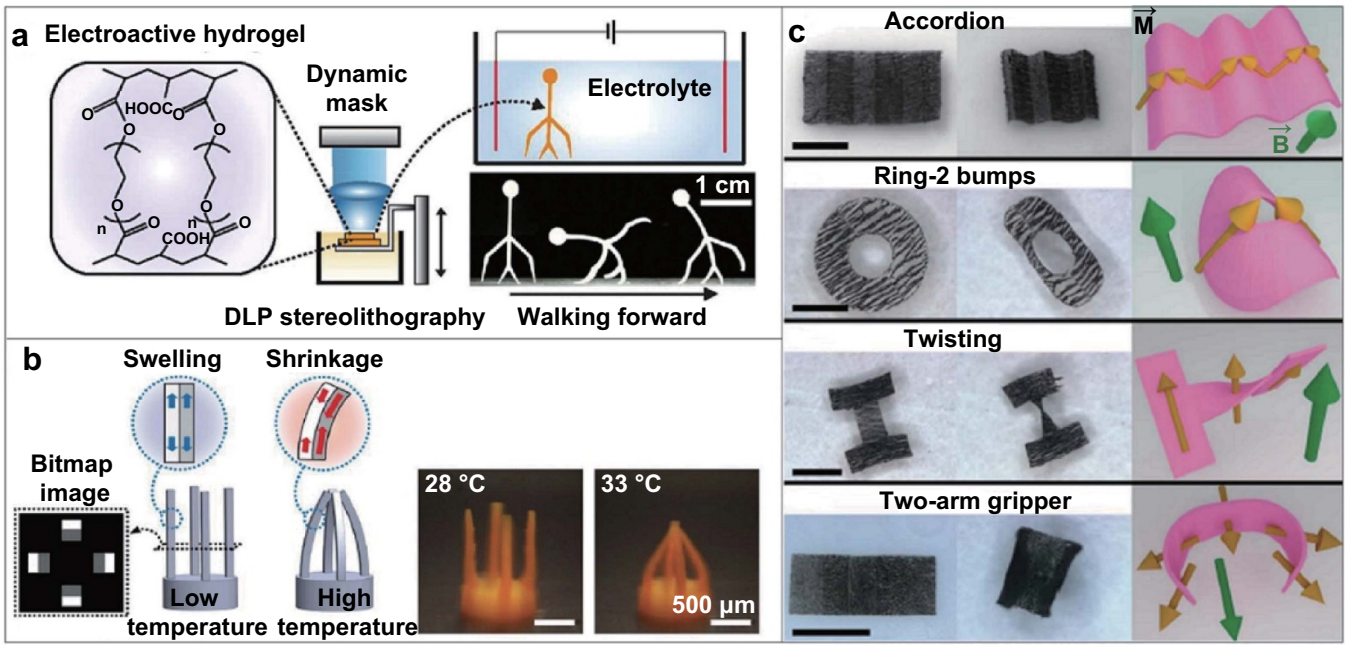

Figure 10. Two-way 4D printing for robotic applications. (a) Soft robots printed by PμSL with electroactive hydrogel. Reprinted with permission from [91]. Copyright (2018) American Chemical Society. (b) PNIPAAm micro gripper consisting of four beams was printed using two different grayscale levels. The difference in the swelling ratio between the two regions caused the beams to bend towards the center at high temperature (scale bar: 500 μm). Reproduced from [92]. CC BY 4.0. (c) Millimeter-scale flexible robots fabricated by magnetic field assisted PμSL 3D printing. Yellow arrows represent the direction of local magnetization, and green arrows represent the direction of the actuating magnetic field. Scale bar is 2 mm. Reproduced with permission from [93].

state, the printed metamaterial structures possess completely different thermo-mechanical behavior which can be tuned by changing temperatures. The mechanical tuneability of the SMP enable the shock absorption of the printed metamaterials upon an impact loading. As shown in figure 9(e), compared to the metamaterial structure at 30 °C, the one at 90 °C absorbs more impact energy as the effective modulus decreases significantly from 20.2 MPa at 30 °C to 0.17 MPa at 90 °C.

The 4D printing realized by SMPs exhibits the so-called 'one-way' actuation. The actuation triggered by the external stimuli is not reversible. The additional actuation requires extra shape programming. This 'one-way' actuation makes the SMP based 4D printing not suitable to the applications such as robots and actuators that require reversible and repeatable motions. Therefore, novel materials that exhibit reversible shape change are desired to realized 'two-way' 4D printing.

Different from SMPs, electroactive hydrogel (EAH) exhibiting large deformation in response to an electric is an ideal material for 'two-way' 4D printing due to its favorable functions such as fast actuation, ease of control as well as biomimetic materials properties. Taking advantage of these features, Han *et al* developed an approach that uses PμSL to print EAH structures exhibiting soft robotic manipulation and locomotion [91]. In order to better understand and control actuation, the authors studied the bending deformation of an EAH with different electrolyte concentrations and under various electric field strengths. Based on the findings, they demonstrated complex soft robotic 3D actuations such as gripping and transporting an object as well as a bidirectional locomotion (figure 10(a)).

Thermal-responsive hydrogels that change physical or chemical properties upon temperature variation are another type of ideal materials for 'two-way' 4D printing. Poly(N-isopropylacrylamide) (PNIPAAm) hydrogels, one of the most widely used thermal-responsive hydrogels, have been used to fabricate soft actuators. Han *et al* developed a method to use high resolution PμSL based 3D printing to fabricate PNIPAAm micro-structures that swell at low temperature and shrink at high temperature [92]. Furthermore, the authors utilized the grayscale printing to encode the bending behavior of PNIPAAm beams, and fabricated a gripper that could reversely open and close at low and high temperatures respectively (figure 10(b)).

Due to the fast response to input signals and the ability to be controlled wirelessly in confined spaces, flexible magnetic materials are great candidate materials for 'two-way' 4D printing that fabricates microrobots for the applications of drug delivery, assisted fertilization, cell culture, as well as noninvasive medical intervention inside the vascular system. To fabricate the microrobots where the discrete in planar 3D magnetization can be precisely patterned, Xu *et al* developed an external magnetic field assisted PμSL 3D printing system to encode 3D magnetization in planar flexible composites at the submillimeter scale [93]. In this method, the premagnetized permanent magnetic particles were first precisely reoriented, and the PμSL 3D printing system was applied to selectively cure UV resin to pattern the local magnetization. They fabricated various microrobots which have different geometries and 3D magnetization profiles with a geometrical feature size of 100 μm by 100 μm, precise magnetization feature

size of 250 μm by 250 μm, and layer thickness of 80 μm. The fabricated millimeter-scale structures exhibit higher-order and multi-axis deformation, large-angle bending, or combined bending and torsion (figure 10(c)).

4.4. Bioinspired engineering materials and structures

Natural composites such as the cortical bones of mammals, the dactyl clubs of peacock mantis shrimp the shells of abalones demonstrate superior mechanical properties by taking advantage of reinforcing particles precisely organized into complex architectures which are frequently linked to the highly ordered heterogeneous reinforcement architectures. The diversity of reinforced composites in nature is far beyond the current composite design and fabrication capabilities, because the current fabrication technologies are unable to control the local orientation of the stiff elements that construct reinforcing architectures [59]. The situation is being changing since the development of multimaterial PμSL where the magnetic or electric field is applied to accurately control the orientation and location of reinforcing particles/fibers.

Yang *et al* developed the electrically assisted 3D printing technology for the fabrication of Bouligand-type structures. Surface modified multiwalled carbon nanotubes (MWCNT-S) was employed to strengthen the mechanical property of the printed artificial structure [60]. As schematically illustrated in figure 11(a), the rotating electric field aligns the MWCNT-S to adjust the mechanical properties of the printed structures. The rotation of 180° is completed by N layers, and the effect of the number of layers on the acted static compression force was investigated. It was found that the maximum load increases with the increasing of the layers. Besides, the authors provided a feasible method for printing artificial meniscus where its local mechanical property can be tuned by adjusting the MWCNT-S alignment. Furthermore, they printed nacre-inspired structures by aligning graphene nanoplatelets (GNs) in the electric field during printing [61]. The GN in the printed layers does not only enhance the mechanical strength (figure 11(b)), but also lowers the electrical resistance of the architecture, because GN exhibits high in-plane rigidity and substantial out-of-plane flexibility, as well as high conductivity. Based on the experimental comparison, the maximum load the artificial nacre can carry is almost the same as the natural one does. In addition, the printed nacre demonstrates anisotropic electrical properties, which can be used for self-sensing in practice.

Martin *et al* developed a '3D magnetic printing' technique that enables the recreation of complex bioinspired reinforced architectures [59]. The authors coated the nonmagnetic reinforcing materials with iron oxide nanoparticles. During printing, the external rotating magnetic field is first applied to align the magnetic nanoparticles, and then PμSL system polymerizes the voxels with aligned particles to solidify the structure and fixing the orientation of the reinforcement. The two steps are repeated until the printing of a layer with different particle orientations is completed. As presented in figure 11(c), the authors successfully fabricated bioinspired structures of artificial Abalone shell, Peacock mantis shrimp, as well as Mammalian cortical bone. It can be seen that those 3D printed structures with programmable alignment of the magnetic nanoparticles demonstrating unique properties of those composite materials on stiffness, strength, toughness and multifunctionality.

Biomimetic functional surfaces, for example, the plant leaves inspired superhydrophobic surfaces have been attracting great attention for various technological applications. However, the traditional manufacturing technologies limit the capability of duplicating the complex hierarchical microstructures. To address this challenge, Yang *et al* developed an immersed surface accumulation based 3D (ISA-3D) printing technique to manufacture eggbeater structure [51]. In order to remove the static charges and increase the surface roughness, multiwalled carbon nanotubes have been added to the liquid resin, leading a fact that the surface of the artificial structure dominated by both of the chemical composition and geometric structures. The condition of water and oil on different surfaces are shown in figure 11(d), indicating that the smooth surface is hydrophilic for both of water and oil, and nanocoating and 3D printed micro pillar enhance the contact angle of the surface, and the 3D printed eggbeater is super-hydrophobic to water, but is still hydrophilic to oil. More interestingly, the water droplet adheres to the eggbeater even rotated for 180°, which is totally different with those hydrophobic surfaces originated from the chemical composition. Due to the advantage of the 3D printing method, the eggbeater can be precisely manufactured. The size and the number of arms can be easily controlled. In addition, the hydrophobicity of the 3D printed structures has been used for the water/oil separation, microreactors, and water transportation. Their work paves a new way for designing artificial hydrophobic surfaces on the basis of the structures, not only the chemical composition itself.

4.5. Biomedical applications

Because of its capabilities of fabricating customized structures in high-resolution and complex geometry, PμSL has also been widely used in biomedical applications such as drug screening, disease study, tissue engineering, central nervous system regeneration, and cell-seeding scaffolds.

To demonstrate the *in vitro* maturation of hiPSC-derived hepatic progenitor cells (hiPSC-HPCs) in a 3D environment that is used to simulate the physiologically relevant cell combination and microarchitecture, Ma *et al* used PμSL to fabricate a 3D hydrogel-based triculture model that embeds hiPSC-HPCs with human umbilical vein endothelial cells and adipose derived stem cells in a microscale hexagonal architecture (figures 12(a)–(c)) [94]. The 3D printed triculture model shows both phenotypic and functional enhancements in the hiPSC-derived hepatic progenitor cells over weeks of *in vitro* culture, including higher liver-specific gene expression levels, improved morphological organization, increased metabolic product secretion, as well as enhanced cytochrome P450 induction. The development of a 3D biomimetic liver model recapitulates the native liver module architecture and shows great potentials for a number of biomedical applications such as disease modeling and early drug screening.

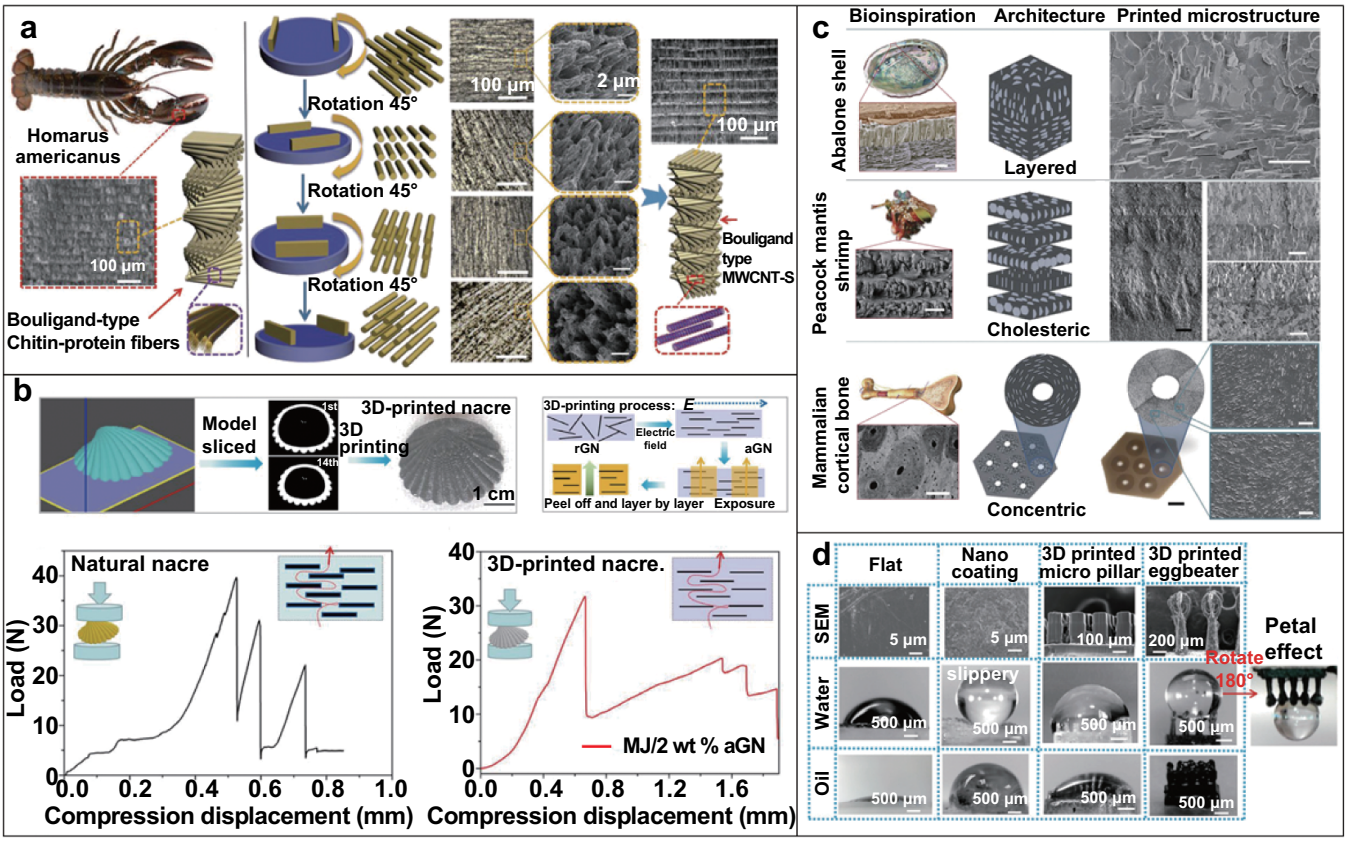

Figure 11. Bioinspired 3D printing. (a) Biomimetic architectures with Bouligand-type MWCNT-S can be recreated by electrically assisted 3D printing. [60] John Wiley & Sons. © 2017 WILEY–VCH Verlag GmbH & Co. KGaA, Weinheim. (b) Electrically assisted 3D printing of nacre-inspired structures with graphene nanoplatelets (GNs). Reproduced with permission from [61]. (c) Bioinspired composites with microstructured architectures can be recreated with 3D magnetic printing. Reproduced from [59]. CC BY 4.0. (d) 3D printed biomimetic super hydrophobic structure for microdroplet manipulation. [51] John Wiley & Sons. © 2018 WILEY–VCH Verlag GmbH & Co. KGaA, Weinheim.

In order to address the low cell adhesion abilities of the traditional UV curable hydrogels such as polyethylene glycol diacrylate (PEGDA) and PEGDA and gelatin methacrylate (GelMA), and to make a natural fibrous protein- silk fibroin (SF) UV curable, Kim *et al* developed a bioink from silk fibroin (SF) that is compatible with PμSL and other DLP based 3D printing [95]. The authors produced the SF-based bioink (Sil-MA) by the methacrylation process of glycidyl methacrylate (GMA). The degree of methacrylation on SF modified with different GMA amounts was evaluated, and the Sil-MA concentration dependent physical and mechanical properties was also characterize. The developed Sil-MA bioink is well-suited for the tissue and organ engineering with PμSL and other DLP based 3D printing, and allows users to build highly complex organ structures, including the heart, vessel, brain, trachea and ear, which are highly structural stable and biocompatible (figure 12(d)).

To study solid organs transport fluids through biophysically and biochemical entangled vascular networks that are biophysically, Grigoryan *et al* used PμSL to fabricate intravascular and multivascular structures by using photo-polymerizable hydrogels added with food dye additives as biocompatible photo-absorbers (figures 12(e)–(g)) [96]. The functional bicuspid valves and efficient intravascular 3D fluid mixers were printed in minutes. The authors further elaborated entangled vascular networks from space-filling mathematical topologies and explore the oxygenation and flow of human red blood cells during tidal ventilation and distension of a proximate airway.

In order to fabricate central nervous system (CNS) structures that consist of complexity of CNS architecture, Koffler *et al* used PμSL to create a complex CNS structure for regenerative medicine applications in the spinal cord (figures 12(h)–(k)) [97]. The authors printed 3D biomimetic hydrogel scaffolds with the tailorable dimensions of the rodent spinal cord that is scalable to human spinal cord sizes and lesion geometries. They tested the ability of 3D-printed scaffolds loaded with neural progenitor cells (NPCs) to support axon regeneration and form new 'neural relay' across sites of complete spinal cord injury *in vivo* in rodents. The research found that injured host axons, regenerate into 3D biomimetic scaffolds and synapse onto NPCs implanted into the device, and that implanted NPCs extend axons out of the scaffold and into the host spinal cord below the injury to restore synaptic transmission and significantly improve functional outcomes.

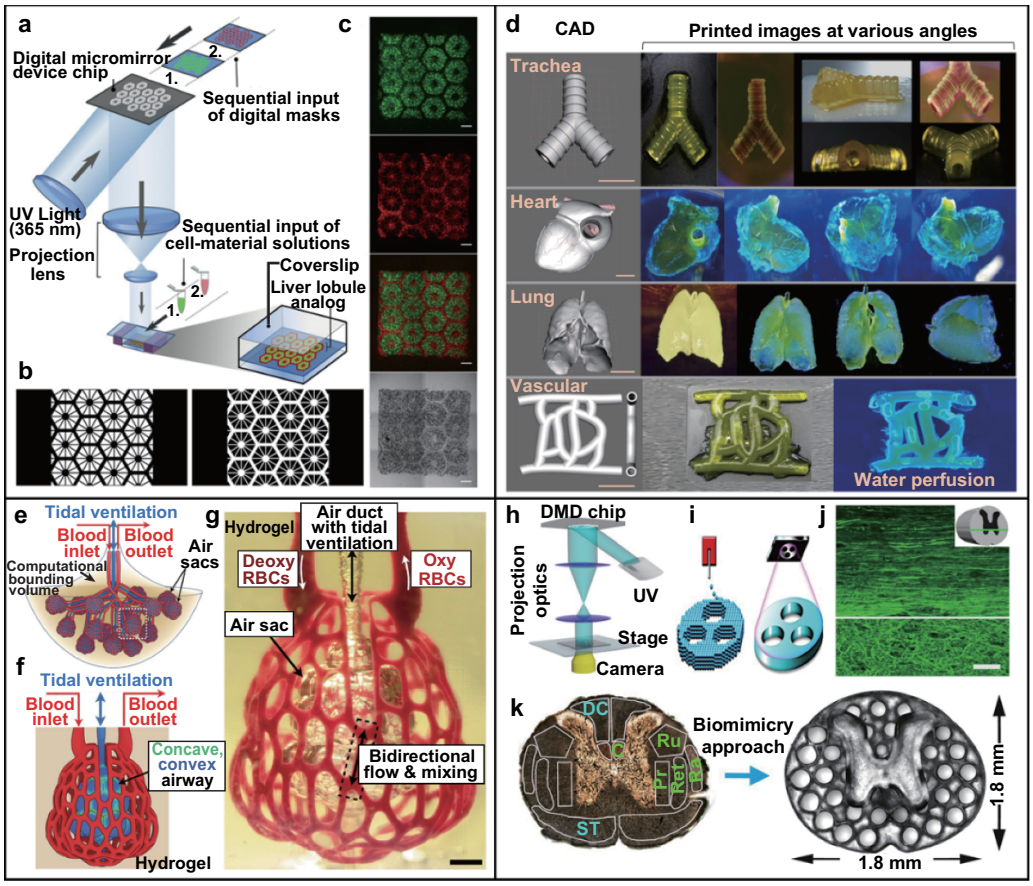

Figure 12. Biomedical applications. (a)–(c) 3D bioprinting of hydrogel based hepatic construct. Reproduced with permission from [94]. (a) Schematic diagram of 3D bioprinting approach. (b) Grayscale digital masks corresponding to polymerizing lobule structure (left) and vascular structure (right). (c) Images taken under fluorescent and bright field channels showing patterns of fluorescently labeled hiPSC-HPCs (green) in 5% (wt/vol) GelMA and supporting cells (red) in 2.5% (wt/vol) GelMA with 1% GMHA on day 0. (scale bars: 500 μm.) (d) 3D printing using silk fibroin bioink (Sil-MA). Trachea, heart, lung, and vessel mimicked shape; (left) CAD images depicting the trachea, heart, lung, and vessel and (right) printed images at various angles. Reproduced from [95]. CC BY 4.0. (e)–(g) Tidal ventilation and oxygenation in hydrogels with vascularized alveolar model topologies. (e) Elaboration of a lung-mimetic design. Reproduced with permission from [96]. (f) The distal lung subunit. (g) Photograph of a printed hydrogel containing the distal lung subunit during RBC perfusion while the air sac was ventilated with O_2 (scale bar, 1 mm). (h)–(k) The 3D-printed scaffold mimics the spinal cord architecture. Reproduced from [97]. CC BY 4.0. (h) 3D-printer setup. (i) Comparison between extrusion-based 3D printing (left) and PμSL based 3D printing (right). (j) Heavy chain neurofilament (NF200) labeling of axons in intact T3 rat spinal cord. (k) Axonal projections in the spinal cord are linearly organized into regions (fascicles) containing axons of related function.

5. Conclusion

This paper reviews the PμSL based 3D printing technologies which are capable of fabricating high-resolution (up to 0.6 μm) and complex 3D architectures covering multiple scales and with multiple materials. This paper aims to summarize the recent development of the PμSL based 3D printing technologies, and the related applications. It introduces the working principle, the commercialized products, and the recent multiscale, multimaterial printing capability of PμSL as well as some functional photopolymers that are suitable to PμSL. This review paper also summarizes a few typical applications of PμSL including mechanical metamaterials, optical components, 4D printing, bioinspired materials and biomedical applications.

Despite of the recent rapid development, the evolution of PμSL into a more powerful 3D printing approach faces the following challenges. (i) Big image data processing and storage. The multiscale printing realized by PμSL does not only require special designs on hardware, but high-efficiency image processing and storage technologies. For example, the printing of a 100 mm$\times$100 mm$\times$60 mm solid with 1 μm resolution requires 2×10^{14} data points. Using traditional slicing technology to slice such a solid results in huge image data in the size of 150 TB. Therefore, without new image processing and storage technologies, PμSL based multiscale 3D printing could not be used in real applications. (ii) Voxel printing. A physical object can be described by a collection of finite volume elements, which is called voxels. Multimaterial voxel 3D printing offers the possibility of fabricating 3D structures where the

material property can be controlled voxel by voxel, and optimizes printed structures by defining the local material composition, structure and properties. Despite of the recent progress, the current multimaterial printing capability is not sufficient for voxel 3D printing in terms of the frequency as well as the channels of material exchange. Therefore, a more powerful multimaterial printing technology is desired to enable the voxel printing on PμSL. (iii) High-resolution ceramic printing. 3D printing ceramic structures has a wide range of applications in aerospace, MEMs, electronics which demand printed ceramic parts in small scales and with high precision. There have been attempts to use DLP or SLA to 3D print ceramic part by either using ceramic particles loaded precursor or polymer derive ceramics. However, the printing high resolution and high density ceramic parts by using PμSL has not yet been achieved due to lack of fundamental studies on the effect of highly viscous ceramic particles loaded precursor on the printing process and resolution as well as limited ceramics can be printing using polymer derive ceramics. In conclusion, once the capabilities of big image data processing, voxel printing as well as ceramics printing are established, PμSL will become a more powerful 3D printing technology which will be more widely adopted by industry.

Acknowledgments

Q G acknowledges the support by the Centers for Mechanical Engineering Research and Education at MIT and SUSTech. Z W acknowledges the support by the National Natural Science Foundation of China (51420105009).

Conflicts of interest

N X F declares financial conflict of interest as cofounder of BMF Materials Inc.

ORCID iD

Qi Ge https://orcid.org/0000-0002-8666-8532

References

[1] Layani M, Wang X F and Magdassi S 2018 Novel materials for 3D printing by photopolymerization *Adv. Mater.* **30** 1706344
[2] Bikas H, Stavropoulos P and Chryssolouris G 2016 Additive manufacturing methods and modelling approaches: a critical review *Int. J. Adv. Manuf. Technol.* **83** 389–405
[3] UPS 2019 3D printing: the next revolution in industrial manufacturing (https://www.ups.com/media/en/3D_Printing_executive_summary.pdf)
[4] Macdonald N P, Cabot J M, Smejkal P, Guijt R M, Paull B and Breadmore M C 2017 Comparing microfluidic performance of three-dimensional (3D) printing platforms *Anal. Chem.* **89** 3858–66
[5] Stratasys Inc 2019 Connex3 objet500 and objet350 (https://www.stratasys.com/3d-printers/objet-350-500-connex3)
[6] BigRep GmbH 2019 Large-scale 3D printer BigRep ONE (https://bigrep.com/bigrep-one/)
[7] Kuang X, Chen K J, Dunn C K, Wu J T, Li V C F and Qi H J 2018 3D printing of highly stretchable, shape-memory, and self-healing elastomer toward novel 4D printing *ACS Appl. Mater. Interfaces* **10** 7381–8
[8] Sydney Gladman A, Matsumoto E A, Nuzzo R G, Mahadevan L and Lewis J A 2016 Biomimetic 4D printing *Nat. Mater.* **15** 413–8
[9] Chen B L, Jiang Y Z, Tang X H, Pan Y Y and Hu S 2017 Fully packaged carbon nanotube supercapacitors by direct ink writing on flexible substrates *ACS Appl. Mater. Interfaces* **9** 28433–40
[10] Le T T, Austin S A, Lim S, Buswell R A, Gibb A G F and Thorpe T 2012 Mix design and fresh properties for high-performance printing concrete *Mater. Struct.* **45** 1221–32
[11] Gosselin C, Duballet R, Roux P, Gaudillière N, Dirrenberger J and Morel P 2016 Large-scale 3D printing of ultra-high performance concrete—a new processing route for architects and builders *Mater. Des.* **100** 102–9
[12] 3D Concrete House Printer 2019 (http://www.totalkustom.com/3d-concrete-printers.html)
[13] Skylar-Scott M A, Mueller J, Visser C W and Lewis J A 2019 Voxelated soft matter via multimaterial multinozzle 3D printing *Nature* **575** 330–5
[14] SLM-Solutions Inc 2019 (www.slm-solutions.com/products/machines/selectivelasermeltingmachine)
[15] TRUMPF Inc 2019 Additive production systems (https://www.trumpf.com/en_US/products/machines-systems/additive-production-systems/)
[16] 3D Systems Inc. 3D printers, 3D scanning, software, manufacturing and healthcare services (https://www.3dsystems.com/)
[17] EOS Inc 2019 Systems and materials for additive manufacturing with metals (www.eos.info/systems_solutions/metal/systems_equipment?_scrivito_display_mode=view&_scrivito_workspace_id=published)
[18] Nanoscribe GmbH 2019 Photonic Professional GT2: world's highest resolution 3D printer (https://www.nanoscribe.com/en/solutions/photonic-professional-gt2)
[19] Kawata S, Sun H B, Tanaka T and Takada K 2001 Finer features for functional microdevices *Nature* **412** 697–8
[20] Takada K, Sun H B and Kawata S 2005 Improved spatial resolution and surface roughness in photopolymerization-based laser nanowriting *Appl. Phys. Lett.* **86** 071122
[21] Xing J F, Dong X Z, Chen W Q, Duan X M, Takeyasu N, Tanaka T and Kawata S 2007 Improving spatial resolution of two-photon microfabrication by using photoinitiator with high initiating efficiency *Appl. Phys. Lett.* **90** 131106
[22] Saha S K, Wang D E, Nguyen V H, Chang Y N, Oakdale J S and Chen S-C 2019 Scalable submicrometer additive manufacturing *Science* **366** 105–9
[23] Zhang X, Jiang X N and Sun C 1999 Micro-stereolithography of polymeric and ceramic microstructures *Sensors Actuators* A **77** 149–56
[24] Wang J, Goyanes A, Gaisford S and Basit A W 2016 Stereolithographic (SLA) 3D printing of oral modified-release dosage forms *Int. J. Pharm.* **503** 207–12
[25] UnionTech Inc. 2019 3D stereolithography printing solutions (http://en.union-tek.com/)
[26] Materialise Inc. 2019 Stereolithography (https://www.materialise.com/en/manufacturing/3d-printing-technology/stereolithography)
[27] Formlabs 2019 Resin library and 3D printing materials (https://formlabs.com/3d-printers/form-3/tech-specs/)

[28] Sun C, Fang N, Wu D M and Zhang X 2005 Projection micro-stereolithography using digital micro-mirror dynamic mask *Sensors Actuators* A **121** 113–20

[29] Zheng X Y, Deotte J, Alonso M P, Farquar G R, Weisgraber T H, Gemberling S, Lee H, Fang N and Spadaccini C M 2012 Design and optimization of a light-emitting diode projection micro-stereolithography three-dimensional manufacturing system *Rev. Sci. Instrum.* **83** 125001

[30] Zheng X Y *et al* 2014 Ultralight, ultrastiff mechanical metamaterials *Science* **344** 1373–7

[31] Zheng X Y *et al* 2016 Multiscale metallic metamaterials *Nat. Mater.* **15** 1100–6

[32] BMF Materials Inc. 2019 Micro 3D printing, industrial micro precision 3D printing (http://www.bmftec.com/)

[33] Gong H, Bickham B P, Woolley A T and Nordin G P 2017 Custom 3D printer and resin for 18 μm $\times$ 20 μm microfluidic flow channels *Lab Chip* **17** 2899–909

[34] Zhang R J and Larsen N B 2017 Stereolithographic hydrogel printing of 3D culture chips with biofunctionalized complex 3D perfusion networks *Lab Chip* **17** 4273–82

[35] Shallan A I, Smejkal P, Corban M, Guijt R M and Breadmore M C 2014 Cost-effective three-dimensional printing of visibly transparent microchips within minutes *Anal. Chem.* **86** 3124–30

[36] Ge Q, Sakhaei A H, Lee H, Dunn C K, Fang N X and Dunn M L 2016 Multimaterial 4D printing with tailorable shape memory polymers *Sci. Rep.* **6** 31110

[37] EnvisionTEC, Inc. 2019 Desktop, professional and industrial 3D printers (https://envisiontec.com/)

[38] Tumbleston J R *et al* 2015 Continuous liquid interface production of 3D objects *Science* **347** 1349–52

[39] Walker D A, Hedrick J L and Mirkin C A 2019 Rapid, large-volume, thermally controlled 3D printing using a mobile liquid interface *Science* **366** 360–4

[40] Wu S H, Serbin J and Gu M 2006 Two-photon polymerisation for three-dimensional micro-fabrication *J. Photochem. Photobiol.* A **181** 1–11

[41] Hull C W 1986 Apparatus for production of three-dimensional objects by stereolithography *US Patent* US4575330A

[42] Reiser A, Lindén M, Rohner P, Marchand A, Galinski H, Sologubenko A S, Wheeler J M, Zenobi R, Poulikakos D and Spolenak R 2019 Multi-metal electrohydrodynamic redox 3D printing at the submicron scale *Nat. Commun.* **10** 1853

[43] Liashenko I, Rosell-Llompart J and Cabot A 2020 Ultrafast 3D printing with submicrometer features using electrostatic jet deflection *Nat. Commun.* **11** 753

[44] Kelly B E, Bhattacharya I, Heidari H, Shusteff M, Spadaccini C M and Taylor H K 2019 Volumetric additive manufacturing via tomographic reconstruction *Science* **363** 1075–9

[45] Loterie D, Delrot P and Moser C 2020 High-resolution tomographic volumetric additive manufacturing *Nat. Commun.* **11** 852

[46] Kowsari K, Akbari S, Wang D, Fang N X and Ge Q 2018 High-efficiency high-resolution multimaterial fabrication for digital light processing-based three-dimensional printing *3D Print. Addit. Manuf.* **5** 185–93

[47] Han D, Yang C, Fang N X and Lee H 2019 Rapid multi-material 3D printing with projection micro-stereolithography using dynamic fluidic control *Addit. Manuf.* **27** 606–15

[48] Xiang Y L, Huang S L, Huang T Y, Dong A, Cao D, Li H, Xue Y, Lv P and Duan H 2020 Superrepellency of underwater hierarchical structures on *Salvinia* leaf *Proc. Natl Acad. Sci. USA* **117** 2282–7

[49] Han D, Morde R S, Mariani S, La Mattina A A, Vignali E, Yang C, Barillaro G and Lee H 2020 4D printing of a bioinspired microneedle array with backward-facing barbs for enhanced tissue adhesion *Adv. Funct. Mater.* **30** 1909197

[50] Wang Y J, Gao L B, Fan S F, Zhou W Z, Li X and Lu Y 2019 3D printed micro-mechanical device (MMD) for *in situ* tensile testing of micro/nanowires *Extreme Mech. Lett.* **33** 100575

[51] Yang Y, Li X J, Zheng X, Chen Z Y, Zhou Q F and Chen Y 2018 3D-printed biomimetic super-hydrophobic structure for microdroplet manipulation and oil/water separation *Adv. Mater.* **30** 1704912

[52] Ge Q, Qi H J and Dunn M L 2013 Active materials by four-dimension printing *Appl. Phys. Lett.* **103** 131901

[53] Ge Q, Dunn C K, Qi H J and Dunn M L 2014 Active origami by 4D printing *Smart Mater. Struct.* **23** 094007

[54] Wang Q M, Jackson J A, Ge Q, Hopkins J B, Spadaccini C M and Fang N X 2016 Lightweight mechanical metamaterials with tunable negative thermal expansion *Phys. Rev. Lett.* **117** 175901

[55] Liu W J *et al* 2017 Rapid continuous multimaterial extrusion bioprinting *Adv. Mater.* **29** 1604630

[56] Zhang B *et al* 2018 Highly stretchable hydrogels for UV curing based high-resolution multimaterial 3D printing *J. Mater. Chem.* B **6** 3246–53

[57] Zhang Y F, Zhang N B, Hingorani H, Ding N Y, Wang D, Yuan C, Zhang B, Gu G and Ge Q 2019 Fast-response, stiffness-tunable soft actuator by hybrid multimaterial 3D printing *Adv. Funct. Mater.* **29** 1806698

[58] Zhang Y F, Ng C J X, Chen Z, Zhang W, Panjwani S, Kowsari K, Yang H Y and Ge Q 2019 Miniature pneumatic actuators for soft robots by high-resolution multimaterial 3D printing *Adv. Mater. Technol.* **4** 1900427

[59] Martin J J, Fiore B E and Erb R M 2015 Designing bioinspired composite reinforcement architectures via 3D magnetic printing *Nat. Commun.* **6** 8641

[60] Yang Y, Chen Z Y, Song X, Zhang Z F, Zhang J, Shung K K, Zhou Q and Chen Y 2017 Biomimetic anisotropic reinforcement architectures by electrically assisted nanocomposite 3D printing *Adv. Mater.* **29** 1605750

[61] Yang Y, Li X J, Chu M, Sun H F, Jin J, Yu K, Wang Q, Zhou Q and Chen Y 2019 Electrically assisted 3D printing of nacre-inspired structures with self-sensing capability *Sci. Adv.* **5** eaau9490

[62] Bagheri A and Jin J Y 2019 Photopolymerization in 3D printing *ACS Appl. Polym. Mater.* **1** 593–611

[63] Wu J T, Zhao Z A, Hamel C M, Mu X M, Kuang X, Guo Z and Qi H J 2018 Evolution of material properties during free radical photopolymerization *J. Mech. Phys. Solids* **112** 25–49

[64] Mu Q Y, Wang L, Dunn C K, Kuang X, Duan F, Zhang Z, Qi H J and Wang T 2017 Digital light processing 3D printing of conductive complex structures *Addit. Manuf.* **18** 74–83

[65] Zhang B, Zhang W, Zhang Z Q, Zhang Y F, Hingorani H, Liu Z, Liu J and Ge Q 2019 Self-healing four-dimensional printing with an ultraviolet curable double-network shape memory polymer system *ACS Appl. Mater. Interfaces* **11** 10328–36

[66] Patel D K, Sakhaei A H, Layani M, Zhang B, Ge Q and Magdassi S 2017 Highly stretchable and UV curable elastomers for digital light processing based 3D printing *Adv. Mater.* **29** 1606000

[67] Zhang B, Kowsari K, Serjouei A, Dunn M L and Ge Q 2018 Reprocessable thermosets for sustainable three-dimensional printing *Nat. Commun.* **9** 1831

[68] Yu K H, Xin A, Du H X, Li Y and Wang Q M 2019 Additive manufacturing of self-healing elastomers *NPG Asia Mater.* **11** 7

[69] Li X P, Yu R, He Y Y, Zhang Y, Yang X, Zhao X and Huang W 2019 Self-healing polyurethane elastomers based on a disulfide bond by digital light processing 3D printing *ACS Macro Lett.* **8** 1511–6

[70] Shelby R A, Smith D R and Schultz S 2001 Experimental verification of a negative index of refraction *Science* **292** 77–9

[71] Parimi P V, Lu W T, Vodo P and Sridhar S 2003 Imaging by flat lens using negative refraction *Nature* **426** 404

[72] Yen T J, Padilla W J, Fang N, Vier D C and Smith D R *et al* 2004 Terahertz magnetic response from artificial materials *Science* **303** 1494–6

[73] Fang N, Xi D J, Xu J Y, Ambati M, Srituravanich W, Sun C and Zhang X 2006 Ultrasonic metamaterials with negative modulus *Nat. Mater.* **5** 452–6

[74] Zhang S, Xia C G and Fang N 2011 Broadband acoustic cloak for ultrasound waves *Phys. Rev. Lett.* **106** 024301

[75] Zhang S, Yin L L and Fang N 2009 Focusing ultrasound with an acoustic metamaterial network *Phys. Rev. Lett.* **102** 194301

[76] Chen X F, Liu W Z, Dong B Q, Lee J, Ware H O T, Zhang H F and Sun C 2018 High-speed 3D printing of millimeter-size customized aspheric imaging lenses with sub 7 nm surface roughness *Adv. Mater.* **30** 1705683

[77] Gissibl T, Thiele S, Herkommer A and Giessen H 2016 Two-photon direct laser writing of ultracompact multi-lens objectives *Nat. Photonics* **10** 554–60

[78] Yuan C, Kowsari K, Panjwani S, Chen Z C, Wang D, Zhang B, Ng C J-X, Alvarado P V Y and Ge Q 2019 Ultrafast three-dimensional printing of optically smooth microlens arrays by oscillation-assisted digital light processing *ACS Appl. Mater. Interfaces* **11** 40662–8

[79] Tibbits S 2013 The emergence of '4D printing' (https://www.ted.com/talks/skylar_tibbits_the_emergence_of_4d_printing)

[80] Mao Y Q, Yu K, Isakov M S, Wu J T, Dunn M L and Jerry Qi H 2015 Sequential self-folding structures by 3D printed digital shape memory polymers *Sci. Rep.* **5** 13616

[81] Wu J T, Yuan C, Ding Z, Isakov M, Mao Y Q, Wang T, Dunn M L and Qi H J 2016 Multi-shape active composites by 3D printing of digital shape memory polymers *Sci. Rep.* **6** 24224

[82] Zarek M, Layani M, Cooperstein I, Sachyani E, Cohn D and Magdassi S 2016 3D printing of shape memory polymers for flexible electronic devices *Adv. Mater.* **28** 4449–54

[83] Yang C, Boorugu M, Dopp A, Ren J, Martin R, Han D, Choi W and Lee H 2019 4D printing reconfigurable, deployable and mechanically tunable metamaterials *Mater. Horiz.* **6** 1244–50

[84] Raviv D *et al* 2015 Active printed materials for complex self-evolving deformations *Sci. Rep.* **4** 7422

[85] Wu D, Song J Q, Zhai Z R, Hua M T, Kim C, Frenkel I, Jiang H and He X 2019 Visualizing morphogenesis through instability formation in 4-D printing *ACS Appl. Mater. Interfaces* **11** 47468–75

[86] Yuan C, Roach D J, Dunn C K, Mu Q Y, Kuang X, Yakacki C M, Wang T J, Yu K and Qi H J 2017 3D printed reversible shape changing soft actuators assisted by liquid crystal elastomers *Soft Matter* **13** 5558–68

[87] Davidson E C, Kotikian A, Li S C, Aizenberg J and Lewis J A 2020 3D printable and reconfigurable liquid crystal elastomers with light-induced shape memory via dynamic bond exchange *Adv. Mater.* **32** 1905682

[88] Zhang C, Lu X L, Fei G X, Wang Z H, Xia H S and Zhao Y 2019 4D printing of a liquid crystal elastomer with a controllable orientation gradient *ACS Appl. Mater. Interfaces* **11** 44774–82

[89] Kotikian A, McMahan C, Davidson E C, Muhammad J M, Weeks R D, Daraio C and Lewis J A 2019 Untethered soft robotic matter with passive control of shape morphing and propulsion *Sci. Robot.* **4** eaax7044

[90] Kuang X, Roach D J, Wu J T, Hamel C M, Ding Z, Wang T, Dunn M L and Qi H J 2019 Advances in 4D printing: materials and applications *Adv. Funct. Mater.* **29** 1805290

[91] Han D, Farino C, Yang C, Scott T, Browe D, Choi W, Freeman J W and Lee H 2018 Soft robotic manipulation and locomotion with a 3D printed electroactive hydrogel *ACS Appl. Mater. Interfaces* **10** 17512–8

[92] Han D, Lu Z C, Chester S A and Lee H 2018 Micro 3D printing of a temperature-responsive hydrogel using projection micro-stereolithography *Sci. Rep.* **8** 1963

[93] Xu T Q, Zhang J C, Salehizadeh M, Onaizah O and Diller E 2019 Millimeter-scale flexible robots with programmable three-dimensional magnetization and motions *Sci. Robot.* **4** eaav4494

[94] Ma X Y *et al* 2016 Deterministically patterned biomimetic human iPSC-derived hepatic model via rapid 3D bioprinting *Proc. Natl Acad. Sci. USA* **113** 2206–11

[95] Kim S H *et al* 2018 Precisely printable and biocompatible silk fibroin bioink for digital light processing 3D printing *Nat. Commun.* **9** 1620

[96] Grigoryan B *et al* 2019 Multivascular networks and functional intravascular topologies within biocompatible hydrogels *Science* **364** 458–64

[97] Koffler J *et al* 2019 Biomimetic 3D-printed scaffolds for spinal cord injury repair *Nat. Med.* **25** 263–9